

Decomposition of Longitudinal Deformations via Beltrami Descriptors

Ho LAW · Chun Yin SIU · Lok Ming LUI

Received: date / Accepted: date

Abstract We present a mathematical model to decompose a longitudinal deformation into normal and abnormal components. The goal is to detect and extract subtle abnormal deformation from periodic motions in a video sequence. It has important applications in medical image analysis. To achieve this goal, we consider a representation of the longitudinal deformation, called the *Beltrami descriptor*, based on quasiconformal theories. The Beltrami descriptor is a complex-valued matrix. Each longitudinal deformation is associated to a Beltrami descriptor and vice versa. To decompose the longitudinal deformation, we propose to carry out the low rank and sparse decomposition of the Beltrami descriptor. The low rank component corresponds to the periodic motions, whereas the sparse part corresponds to the abnormal motions of a longitudinal deformation. Experiments have been carried out on both synthetic and real video sequences. Results demonstrate the efficacy of our proposed model to decompose a longitudinal deformation into regular and irregular components.

Keywords Longitudinal Deformation, Beltrami Descriptor; Low-rank, sparse, quasiconformal

1 Introduction

Deformation analysis plays a significant role in medical image analysis[58, 45]. Given a longitudinal medical image sequence, the spatio-temporal analysis can be carried out through studying deformations between images, which is useful to understand the pathology for disease analysis. In particular, this paper aims to filter out normal longitudinal deformations from the abnormal which could be caused by certain diseases in a medical video. By normal deformations, we refer to a series of deformations that follows a periodic motion. Suppose there is a medical footage that records a periodic motion, for instance, a beating heart under a normal cardiac motion. Then the normal deformation is this periodic motion. On the other hand, some patients may occasionally suffer from some diseases like Premature Atrial Contraction and Premature Ventricular Contraction that would perturb this kind of normal cardiac deformation[19]. In this case, we call this kind of perturbations the abnormal deformation. Our goal is to extract the abnormal deformation (perturbations) from the normal (periodic) deformation, which are originally combined together. In order to analyze the deformities efficiently and accurately, the capability to decompose a longitudinal deformation into regular and

HKRGC GRF (Project ID:2130549, Reference ID: 14306917), CUHK Direct Grant (Project ID: 4053292)

Ho LAW
The Chinese University of Hong Kong
E-mail: hlwab@connect.ust.hk

Chun Yin SIU
Cornell University
E-mail: cs2323@cornell.edu

Lok Ming LUI
The Chinese University of Hong Kong
E-mail: lmlui@math.cuhk.edu.hk

irregular motions is necessary. For instance, during normal cycles of contraction and expansion of a lung when breathing, some parts of the lung may tremble unnaturally[15]. Combined with the normal motion, doctors might have difficulty to discern the abnormal motion. It thus calls for the need of a mathematical model to the decomposition of longitudinal deformation into normal and abnormal components.

To achieve this goal, an effective representation of the longitudinal deformation is necessary. An intuitive representation is based on the deformation vector fields obtained via image registration techniques. As vector fields cannot effectively capture the geometric information of deformations, the decomposition based on vector fields is usually unable to extract meaningful regular and irregular components and evidence will be provided in later section. The difficulty is that the extracted components are not in a bijective correspondence with flips or overlaps, which are unnatural and unrealistic for deformations of anatomical structures. In this work, we propose to consider a representation of the longitudinal deformation, called the *Beltrami descriptor*, in quasiconformal theories[14, 34, 6]. The Beltrami descriptor is a complex-valued matrix, which captures the geometric information of the longitudinal deformation. Hence, the geometric distortion and bijectivity of the deformation can be easily controlled[26]. More importantly, it is an effective representation since each longitudinal deformation is associated to a unique Beltrami descriptor and vice versa. The associated deformation is also stable under the perturbation of the descriptor. As such, the manipulation of the longitudinal deformations through the Beltrami descriptors is not sensitive to the error of the descriptors, which is crucial for the decomposition. To decompose the longitudinal deformation, we propose to extract the low rank part and sparse part of the Beltrami descriptor. The periodic motion of the deformation is characterized by the low rank component of the descriptor. On the other hand, abnormal deformation is characterized by the sparse part of the Beltrami descriptor. This low rank and sparse pursuit problem can be relaxed to a complex-valued Robust Principal Component Analysis (RPCA) problem[2, 3], which can be solved by alternating minimization method with multipliers (ADMM)[54]. We test our proposed model on both synthetic and real video sequences. Experimental results illustrate the efficacy of our proposed method for the decomposition of longitudinal deformations.

In short, our contributions of this paper are three-folded.

1. First, we propose to consider a special representation of longitudinal deformations, called the Beltrami descriptor, to decompose the deformation. The Beltrami descriptor captures the geometric information of the deformation, and hence manipulating the descriptor allows us to process and analyze the deformation according to its geometry.
2. Secondly, we consider the low rank and sparse decomposition of the Beltrami descriptor to the decomposition of longitudinal deformation into regular and irregular components. To the best of our knowledge, it is the first work to the decomposition of longitudinal deformation via low rank and sparse pursuit.
3. Thirdly, in practical applications, it is often desirable to extract bijective irregular longitudinal component, which detect and capture the abnormal deformation from normal periodic motion. In this work, we theoretically show that the extracted irregular component is bijective under a suitable choice of parameters.

The paper is organized as follow: in section 2, we will briefly review some previous works related to this paper. In section 3, some necessary mathematical tools will be described. The Beltrami descriptor and our proposed decomposition algorithm will be explained in details in section 4. Last but not least, experimental results will be shown in section 5, and we cap off with a conclusion and discussion of future works in section 6.

2 Previous Work

Shape analysis of structures from images plays a fundamental role in various fields, such as computer visions and medical image analysis. One commonly used approach is based on the analysis of the deformation fields between corresponding images. Deformation fields between images are often obtained through the image registration process. Registration aims to establish a meaningful one-to-one dense correspondence between images. Over years, various registration methods have

been proposed, which can be categorized into feature-based [52, 21, 27, 35], intensity-based [49, 1], and combined-feature-intensity-based methods [51, 26, 37]. Amongst these methods, quasiconformal-based registration models have been widely used [37, 27, 43, 32, 36, 26, 50, 38, 10, 35], with which our model in this paper is built upon. For instance, in [26], Lam et al. proposed an optimization model based on quasiconformal geometry to obtain landmark-based and intensity-based registration between images or surfaces.

Once the deformation fields are obtained, different shape analysis methods have been recently proposed. In [32, 33, 34, 9, 25, 5, 8, 55, 39, 7], Lui et al. proposed to detect shape variation based on the Beltrami coefficients of the deformation field as well as the curvature mismatching. The method has been applied for Alzheimer’s disease analysis [5] and tooth morphometry [9]. A quasiconformal metric for deformation classification is also introduced to classify the left ventricle deformations of myopathic and control subjects [46]. The wavelet support vector machine (WSVM) has been proposed to study the deformation field [42]. Algorithms to analyze deformation field with different geometric scales and directions have also been recently developed. The basic idea is to decompose the vector field representing the deformation into various meaningful components. For instance, Tong et al. [48] proposed a variational model to decompose a vector field into the divergence-free part, the curl-free part, and the harmonic part using the idea of Helmholtz-Hodge decomposition. Recently, the morphlet transform has been proposed to obtain a multi-scale representation for diffeomorphisms [23]. Wavelet transform on the Beltrami coefficient of the deformation field has also been proposed to decompose a deformation into multiple components with various geometric scales [25]. However, to the best of our knowledge, an effective method to analyze time-dependent longitudinal deformation is still lacking.

In this work, our goal is to decompose a longitudinal deformation into normal and abnormal components. To do so, Robust Principal Component Analysis (RPCA) will be performed on the descriptor of the longitudinal deformation. RPCA has been widely studied in recent years and have been used for various applications. For example, Zhou et al. [56] proposed “GoDec” that was adding one more noise term, so as to remove the noise captured by cameras. Also, Zhou et al. [57] made an improvement by imposing one more constraint to ensure the moving objects are small and continuous pieces. Li et al. [29] suggested another method, SSC-RPCA, that could work well when the background exhibits some minor motion, like flowing water of a lake or a river, or the moving object does not move fast enough, with more terms into the original RPCA model to force the model to group different regions of the moving object in a roughly segmented video. Oreifej et al. [41] presented another term to model turbulence to capture moving object in a badly turbulence-corrupted video. Sobral et al. [44] proposed a way to improve detection of moving object by imposing shape constraints. Javed et al. [22] put forward a superpixel-based matrix decomposition method with maximum norm regularizations and structured sparsity constraints to deal with the real-time challenge. The model designed by Ebdai et al. [11] estimates the support of the foreground regions with a superpixel generation step, and then spatial coherence can be imposed. Cao et al. [4] presented a novel method of RPCA, using tensor decomposition, as well as 3D total variation to enforce spatio-temporal continuity of the moving objects.

To compute the RPCA effectively, various numerical methods have been proposed. For example, Lin et al. [31] compared two methods: accelerated proximal gradient algorithm applied to the primal and gradient algorithm applied to the dual problem. Another well-know optimization method, which is going to be used in this paper, is the **Alternating Direction Method (ADM)** proposed by Yuan et al. [54], or similarly the Augmented Lagrange Multiplier Method proposed by Lin et al. [30].

3 Mathematical Background

In this section, we will review some mathematical background related to this work.

3.1 Quasiconformal theories

In the following, some basic ideas of quasiconformal geometry are discussed. For details, we refer readers to [14, 28].

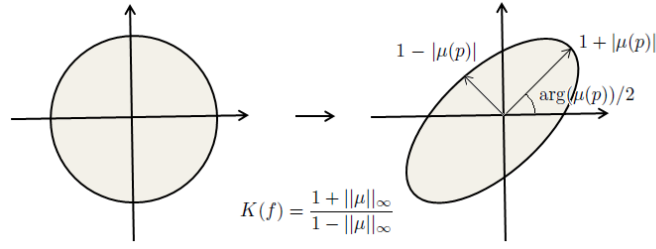


Fig. 1: Illustration of how the Beltrami coefficient determines the conformality distortion.

A surface S with a conformal structure is called a *Riemann surface*. Conformal structure on a Riemann surface, S , is an equivalence class of metrics.

$$[h] = \{e^{2u}h \mid u \in C^\infty(S)\}, \quad (1)$$

where h is some Riemannian metric on S . Given two Riemann surfaces M and N , a map $f : M \rightarrow N$ is *conformal* if it preserves the surface metric up to a multiplicative factor called the *conformal factor*. An immediate consequence is that every conformal map preserves angles. With the angle-preserving property, a conformal map effectively preserves the local geometry of the surface structure. A generalization of conformal maps is the *quasiconformal* maps, which are orientation preserving homeomorphisms between Riemann surfaces with bounded conformality distortion, in the sense that their first order approximations take small circles to small ellipses of bounded eccentricity [14]. Mathematically, $f : \mathbb{C} \rightarrow \mathbb{C}$ is quasiconformal provided that it satisfies the Beltrami equation:

$$\frac{\partial f}{\partial \bar{z}} = \mu(z) \frac{\partial f}{\partial z}. \quad (2)$$

for some complex-valued function μ satisfying $\|\mu\|_\infty < 1$, where μ is called the *Beltrami coefficient*, which is a measure of non-conformality. More precisely, it measures how far the map at each point is deviated from a conformal map. In particular, the map f is conformal around a small neighborhood of p when $\mu(p) = 0$. When $\mu(z) \equiv 0$, the Beltrami's equation becomes the Cauchy-Riemann equation and so the map is a conformal map. As such, a quasiconformal map can be regarded as a generalization of conformal map that allows bounded conformality distortions. Infinitesimally, around a point p , f may be expressed with respect to its local parameter as follows:

$$\begin{aligned} f(z) &= f(p) + f_z(p)z + f_{\bar{z}}(p)\bar{z} \\ &= f(p) + f_z(p)(z + \mu(p)\bar{z}). \end{aligned} \quad (3)$$

Obviously, f is not conformal if and only if $\mu(p) \neq 0$. Locally, f may be considered as a map composed of a translation to $f(p)$ together with a stretch map $S(z) = z + \mu(p)\bar{z}$, which is composed by a multiplication of $f_z(p)$, which is conformal. All the conformal distortion of $S(z)$ is caused by $\mu(p)$. $S(z)$ is the map that causes f to map a small circle to a small ellipse. From $\mu(p)$, we can determine the angles of the directions of maximal magnification and shrinking and the amount of them as well. Specifically, the angle of maximal magnification is $\arg(\mu(p))/2$ with magnifying factor $1 + |\mu(p)|$; the angle of maximal shrinking is the orthogonal angle $(\arg(\mu(p)) - \pi)/2$ with shrinking factor $1 - |\mu(p)|$. Thus, the Beltrami coefficient μ gives us lots of information about the properties of the map (see Figure 1).

The maximal dilation of f is given by:

$$K(f) = \frac{1 + \|\mu\|_\infty}{1 - \|\mu\|_\infty}. \quad (4)$$

Given a Beltrami coefficient $\mu : \mathbb{C} \rightarrow \mathbb{C}$ with $\|\mu\|_\infty < 1$. There always exists a quasiconformal mapping from \mathbb{C} onto itself which satisfies the Beltrami equation in the distributions sense [14]. More precisely, we have the following theorem:

Theorem 1 (Measurable Riemann Mapping Theorem) *Suppose $\mu : \mathbb{C} \rightarrow \mathbb{C}$ is Lebesgue measurable satisfying $\|\mu\|_\infty < 1$, then there exists a quasiconformal homeomorphism ϕ from \mathbb{C} onto itself, which belongs to the Sobolev space $W^{1,2}(\mathbb{C})$ and satisfies the Beltrami Equation (2) in the distributions sense. Furthermore, by fixing $0, 1$ and ∞ , the associated quasiconformal homeomorphism ϕ is uniquely determined.*

Theorem 1 suggests that under a suitable normalization, a homeomorphism from \mathbb{C} or \mathbb{D} onto itself can be uniquely determined by its associated Beltrami coefficient.

3.2 Robust Principal Component Analysis (RPCA)

The RPCA problem is stated as follow: Suppose we are given a matrix $M \in \mathbb{R}^{m \times n}$. Then we would like to solve the following minimisation problem:

$$\min_{\mathcal{N}, \mathcal{A}} \text{rank}(\mathcal{N}) + \alpha \|\mathcal{A}\|_0, \text{ such that } M = \mathcal{N} + \mathcal{A}; \quad (5)$$

where \mathcal{N} and \mathcal{A} are supposed to be a low-rank and a sparse matrix respectively, and α a parameter describing the trade off between the rank of the low-rank matrix and the L_0 norm of the sparse matrix. Since the above problem is NP-hard, we make appeal to a common relaxation, namely:

$$\min_{\mathcal{N}, \mathcal{A}} \|\mathcal{N}\|_* + \alpha \|\mathcal{A}\|_1, \text{ such that } M = \mathcal{N} + \mathcal{A} \quad (6)$$

Given that Equation (6) is a convex optimization problem, the ADM approach suggested by Yuan et. al. [54] is a suitable method. Namely, the Augmented Lagrangian function of Equation (6) is:

$$\mathcal{L}(\mathcal{N}, \mathcal{A}, Z; M) = \|\mathcal{N}\|_* + \alpha \|\mathcal{A}\|_1 - \langle Z, \mathcal{N} + \mathcal{A} - M \rangle + \frac{\beta}{2} \|\mathcal{N} + \mathcal{A} - M\|_2^2 \quad (7)$$

where Z is the multiplier of the linear constraint, β is the penalty parameter. Here, we use $\langle \cdot, \cdot \rangle$ to denote the trace inner product. A simple iterative scheme is as follow:

$$\begin{cases} \mathcal{N}^{k+1} = \arg \min_{\mathcal{N} \in \mathbb{R}^{m \times n}} \mathcal{L}(\mathcal{N}, \mathcal{A}^k, Z^k; M) \\ \mathcal{A}^{k+1} = \arg \min_{\mathcal{A} \in \mathbb{R}^{m \times n}} \mathcal{L}(\mathcal{N}^{k+1}, \mathcal{A}, Z^k; M) \\ Z^{k+1} = Z^k - \beta(\mathcal{N}^{k+1} + \mathcal{A}^{k+1} - M) \end{cases} \quad (8)$$

[54, 40, 2, 47] showed that there are closed formulas to update $\mathcal{N}^{k+1}, \mathcal{A}^{k+1}$ and, obviously, Z^{k+1} at each step. To solve for \mathcal{A}^{k+1} , we can use the explicit solution:

$$\mathcal{A}^{k+1} = \frac{1}{\beta} Z^k - \mathcal{N}^k + M - P_{\Omega_\infty^{\alpha/\beta}} \left(\frac{1}{\beta} Z^k - \mathcal{N}^k + M \right) \quad (9)$$

where $P_{\Omega_\infty^{\alpha/\beta}}$ denoted the Euclidean projection onto $\Omega_\infty^{\alpha/\beta} := \{X \in \mathbb{R}^{n \times n} \mid -\alpha/\beta \leq X_{ij} \leq \alpha/\beta\}$. For the subproblem \mathcal{N}^{k+1} , the explicit solution is

$$\mathcal{N}^{k+1} = U^{k+1} \text{diag} \left(\max\{\sigma_i^{k+1} - \frac{1}{\beta}, 0\} \right) (V^{k+1})^T \quad (10)$$

where $U^{k+1}, V^{k+1}, \sigma_i^{k+1}$ are obtained by SVD that is:

$$M - \mathcal{A}^{k+1} + \frac{1}{\beta} Z^k = U^{k+1} \Sigma^{k+1} (V^{k+1})^T \quad \text{with} \quad \Sigma^{k+1} = \text{diag}(\{\sigma_i^{k+1}\}_{i=1}^r) \quad (11)$$

4 Decomposition of Longitudinal Deformations

In this section, we explain our proposed main algorithm for the decomposition of longitudinal deformations. The goal is to separate abnormal deformations from normal deformations. To achieve this goal, it is necessary to have an effective representation of longitudinal deformations. The longitudinal deformation has to be easily restored from the corresponding representation. In addition, an effective algorithm to decompose the representation is also required.

4.1 Representation of longitudinal deformations.

In this work, we consider to represent the longitudinal deformations based on quasiconformal theories. An effective representation of longitudinal deformations should satisfy the following criteria.

1. First, the representation should capture the geometric information about the deformations. More precisely, it should describe the local geometric distortions created by the deformation mappings, so that the decomposed result should contain information about geometric distortion.
2. The corresponding longitudinal deformations can be restored from the representation by Linear Beltrami Solver(LBS) which will be detailed in later section, so that the deformation fields can be obtained after the decomposition of the representation is carried out.
3. The bijectivity of the corresponding deformations can be controlled during the manipulation of the representation with theoretical support. In other words, the corresponding deformations will not be severely corrupted during the decomposition process of the representation.

To achieve these objectives, we will consider a longitudinal deformation matrix based on the Beltrami coefficients. Suppose $\{I_i\}_{i=1}^t$ are the video frames, each of size $m \times n$, capturing the longitudinal data. Let I_{ref} be a reference image. For each frame I_j , we compute the image registration $f_j : \Omega \rightarrow \Omega$ from I_{ref} to I_j . Here, Ω refers to the rectangular image domain. The image registration can be computed using existing registration algorithms. In this work, the quasiconformal image registration method is applied.

Note that the image domain Ω is discretized into uniformly distributed pixels. As such, we can consider that Ω is discretized by regular triangulation $\{V, E, F\}$, where V is the collection of vertices given by pixels. E and F are the collections of edges and faces respectively. With these notations, we assume $f_i := (\mathbf{u}_i, \mathbf{v}_i)$, where $\mathbf{u}_i : V \rightarrow \mathbb{R}$ and $\mathbf{v}_i : V \rightarrow \mathbb{R}$ are the coordinate functions defined on every vertices. f_i is regarded as piecewise linear on each face. The quasiconformality or local geometric distortion of f_i can then be measured by the Beltrami coefficient.

For the piecewise linear map f_i , we compute its Beltrami Coefficient by the approximation of its partial derivatives on each face $T \in F$. The restriction of f_i on each face T can be written as

$$f_i|_T(x, y) = \begin{pmatrix} a_T x + b_T y + r_T \\ c_T x + d_T y + q_T \end{pmatrix} \quad (12)$$

Hence, $D_x f_i(T) = a_T + i c_T$ and $D_y f_i(T) = b_T + i d_T$. Then the gradient $\nabla_T f_i$ can be obtained by solving:

$$\begin{pmatrix} v_1 - v_0 \\ v_2 - v_0 \end{pmatrix} \begin{pmatrix} a_T & b_T \\ c_T & d_T \end{pmatrix} = \begin{pmatrix} \mathbf{u}(v_1) - \mathbf{u}(v_0) & \mathbf{u}(v_2) - \mathbf{u}(v_0) \\ \mathbf{v}(v_1) - \mathbf{v}(v_0) & \mathbf{v}(v_2) - \mathbf{v}(v_0) \end{pmatrix} \quad (13)$$

where v_0, v_1 and v_2 are the three vertices of the face T . By solving the above linear system, a_T, b_T, c_T, d_T can be computed. And the Beltrami coefficient of f_i on T can be obtained by

$$\mu_i(T) = \frac{(a_T - d_T) + i(c_T + b_T)}{(a_T + d_T) + i(c_T - b_T)} \quad (14)$$

We thus have the following definition of longitudinal deformation descriptor to represent the longitudinal deformations.

Definition 1 (Longitudinal deformation descriptor) With the notations above, the longitudinal deformation descriptor \mathcal{L}^μ for $\{f_i\}_{i=1}^t$ is a $mn \times t$ complex-valued matrix given by

$$\mathcal{L}^\mu = \begin{pmatrix} | & | & & | \\ \mu_1 & \mu_2 & \cdots & \mu_t \\ | & | & & | \end{pmatrix} \quad (15)$$

\mathcal{L}^μ is formulated using Beltrami coefficients, which capture the local geometric distortions under the longitudinal deformations. As it will be explained in the next subsection, \mathcal{L}^μ has a one-one correspondence with the longitudinal deformations. In other words, given \mathcal{L}^μ , the associated longitudinal deformations can be reconstructed. On the other hand, according to quasiconformal theories, the deformation f_j is bijective (or folding-free) if $\|\mu_j\|_\infty < 1$.

4.2 Reconstruction of longitudinal deformations from descriptors.

In the last subsection, we introduce the descriptor \mathcal{L}^μ to represent the longitudinal deformations. In order to utilize the descriptor, a reconstruction algorithm from the descriptor to the corresponding longitudinal deformations is necessary.

Let's discuss how the longitudinal deformations can be reconstructed from \mathcal{L}^μ . Consider $f_j|_T$ restricted to a triangle $T \in F$. Suppose the three vertices of T is given by v_0, v_1 and v_2 , whose coordinates are given by $v_k = (g_k, h_k)$ for $k = 0, 1$ or 2 . v_0, v_1 and v_2 are deformed by $f_j|_T$ to w_0, w_1 and w_2 , whose coordinates are given by $w_k = (s_k, t_k)$ for $k = 0, 1, 2$. Denote $\mu_j(T) = \rho_j + i\tau_j$. Let $\gamma_1(T) = \frac{(\rho_T - 1)^2 + \tau_T^2}{1 - \rho_T^2 - \tau_T^2}$, $\gamma_2(T) = \frac{-2\tau_T}{1 - \rho_T^2 - \tau_T^2}$ and $\gamma_3(T) = \frac{(1 + \rho_T)^2 + \tau_T^2}{1 - \rho_T^2 - \tau_T^2}$.

By comparing the real and imaginary parts, Equation (13) can be formulated as follows:

$$\begin{aligned} a_T &= \alpha_T^0 s_0 + \alpha_T^1 s_1 + \alpha_T^2 s_2; \\ b_T &= \beta_T^0 s_0 + \beta_T^1 s_1 + \beta_T^2 s_2; \\ c_T &= \alpha_T^0 t_0 + \alpha_T^1 t_1 + \alpha_T^2 t_2; \\ d_T &= \beta_T^0 t_0 + \beta_T^1 t_1 + \beta_T^2 t_2. \end{aligned} \tag{16}$$

where

$$\begin{aligned} \alpha_T^0 &= (h_2 - h_3)/\mathcal{A}_T; \alpha_T^1 = (h_2 - h_0)/\mathcal{A}_T; \alpha_T^2 = (h_0 - h_1)/\mathcal{A}_T; \\ \beta_T^0 &= (g_2 - g_3)/\mathcal{A}_T; \beta_T^1 = (g_2 - g_0)/\mathcal{A}_T; \beta_T^2 = (g_0 - g_1)/\mathcal{A}_T; \end{aligned} \tag{17}$$

Here, \mathcal{A}_T refers to the area of T . According to computational Quasiconformal Teichmüller Theory [14], a_T, b_T, c_T and d_T also satisfy the following linear equations:

$$\begin{aligned} \sum_{T \in N_i} \alpha_T^i [\gamma_1(T) a_T + \gamma_2(T) b_T] + \beta_T^i [\gamma_2(T) a_T + \gamma_3(T) b_T] &= 0; \\ \sum_{T \in N_i} \alpha_T^i [\gamma_1(T) c_T + \gamma_2(T) d_T] + \beta_T^i [\gamma_2(T) c_T + \gamma_3(T) d_T] &= 0; \end{aligned} \tag{18}$$

where N_i denotes the set of faces attached to the vertex v_i . Combining Equation (18) and (20), we obtain a linear system to solve for the coordinate functions \mathbf{u}_j and \mathbf{v}_j of f_j , subject to a given boundary condition. In practice, we usually set f_j to be an identity map on the boundary as the boundary condition. Hence, we have $D_j f_j = D_j(\mathbf{u}_j, \mathbf{v}_j) = (\mathbf{b}_j^1, \mathbf{b}_j^2)$, where D_j is a $mn \times mn$ matrix D_j and $(\mathbf{b}_j^1, \mathbf{b}_j^2)$ is a $mn \times 2$ matrix given by the above non-singular linear system.

In summary, given \mathcal{L}^μ , one can reconstruct the longitudinal deformations via solving a big linear system:

$$\tilde{D}\mathbf{f} = \begin{pmatrix} D_1 & & & \\ & D_2 & & \\ & & \ddots & \\ & & & D_t \end{pmatrix} \begin{pmatrix} f_1 \\ f_2 \\ \vdots \\ f_t \end{pmatrix} = \begin{pmatrix} | & | \\ \mathbf{b}^1 & \mathbf{b}^2 \\ | & | \end{pmatrix} := \mathbf{b} \tag{19}$$

where \tilde{D} is a $mnt \times mnt$ block diagonal matrix, where t is the number of frames, and hence the linear system can be solved in parallel, subject to the Dirichlet boundary condition that the map is an identity map on the boundary.

The above discussion gives rise to the following theorem about the relationship between the longitudinal deformation and its associated descriptors.

Theorem 2 *Let denote the longitudinal deformations by \mathbf{f} . To \mathbf{f} is associated with a unique descriptor \mathcal{L}^μ , given by Equation (13), that satisfies $\|\mathcal{L}^\mu\|_\infty < 1$. Conversely, given a descriptor \mathcal{L}^μ of a longitudinal deformation, the corresponding longitudinal deformation \mathbf{f} can be exactly reconstructed and is unique. In other words, if a longitudinal deformation \mathbf{g} has a descriptor given by \mathcal{L}^μ , then $\mathbf{f} = \mathbf{g}$.*

On the other hand, the bijectivity of the longitudinal deformation can be easily controlled by the norm of its descriptor. It can be explained by the following theorem.

Theorem 3 *If $\|\mathcal{L}^\mu\|_\infty < 1$, then its associated longitudinal deformation is bijective.*

Proof Note that $\|\mathcal{L}^\mu\|_\infty = \max_{i,j} \{ |(\mathcal{L}^\mu)_{ij}| \}$, where $(\mathcal{L}^\mu)_{ij}$ denotes the i -th row and j -th column entry of \mathcal{L}^μ . Since $\|\mathcal{L}^\mu\|_\infty < 1$, we have $\|\mu_j\|_\infty < 1$ for all $j = 1, 2, \dots, l$. For every triangular face T , the restriction map $f_j|_T$ on T is a linear map. The Jacobian J_T of $f_j|_T$ is given by

$$J_T = \left| \frac{\partial}{\partial z} (f_j|_T) \right|^2 - \left| \frac{\partial}{\partial \bar{z}} (f_j|_T) \right|^2 = \left| \frac{\partial}{\partial z} (f_j|_T) \right|^2 (1 - |\mu_j(T)|^2) > 0$$

since $|\mu_j(T)| = \left| \frac{\partial f_j|_T}{\partial \bar{z}} \right| / \left| \frac{\partial f_j|_T}{\partial z} \right| < 1$ and $\left| \frac{\partial}{\partial z} (f_j|_T) \right| > 0$ for a well-defined μ_j . we conclude that $f_j|_T$ is orientation-preserving. Thus the piecewise linear deformation f_j is locally injective on every one-ring neighborhood of a vertex. By Hadamard theorem, f_j is globally bijective for all $j = 1, 2, \dots, l$. We conclude that the longitudinal deformation associated to \mathcal{L}^μ is bijective.

In addition, it is important to understand how the difference in two descriptors related to the difference in their corresponding longitudinal deformations.

Theorem 4 *Let \mathcal{L}_1^μ and \mathcal{L}_2^μ be the descriptors of two longitudinal deformations \mathbf{f} and \mathbf{g} respectively. Suppose $\|\mathcal{L}_1^\mu - \mathcal{L}_2^\mu\|_F < \epsilon$, where $\|\cdot\|_F$ denotes the Frobenius norm. Then:*

$$\begin{aligned} \|\mathbf{f} - \mathbf{g}\|_F &< C_1 \epsilon \\ \|\mathcal{D}\mathbf{f} - \mathcal{D}\mathbf{g}\|_F &< C_2 \epsilon \end{aligned} \tag{20}$$

for some positive constants C_1 and C_2 . Here,

$$\mathcal{D}\mathbf{f} = \begin{pmatrix} | & | & | & | & \cdots & | & | \\ \mathcal{D}_1 f_1 & \mathcal{D}_2 f_1 & \mathcal{D}_1 f_2 & \mathcal{D}_2 f_2 & \cdots & \mathcal{D}_1 f_t & \mathcal{D}_2 f_t \\ | & | & | & | & & | & | \end{pmatrix} \in M_{|F| \times 2t}$$

where $\mathcal{D}_1 \varphi = \begin{pmatrix} \frac{\partial \varphi}{\partial z}(T_1) \\ \vdots \\ \frac{\partial \varphi}{\partial z}(T_{|F|}) \end{pmatrix} \in \mathbb{C}^{|F|}$ and $\mathcal{D}_2 \varphi = \begin{pmatrix} \frac{\partial \varphi}{\partial \bar{z}}(T_1) \\ \vdots \\ \frac{\partial \varphi}{\partial \bar{z}}(T_{|F|}) \end{pmatrix} \in \mathbb{C}^{|F|}$, where φ is a piecewise linear map on Ω and $T_j \in F$ is a triangular face. $\mathcal{D}\mathbf{g}$ is defined similarly.

Proof Denote $\mathbf{f} = \begin{pmatrix} | & | & \cdots & | \\ f_1 & f_2 & \cdots & f_t \\ | & | & & | \end{pmatrix}$, $\mathbf{g} = \begin{pmatrix} | & | & \cdots & | \\ g_1 & g_2 & \cdots & g_t \\ | & | & & | \end{pmatrix}$, $\mathcal{L}_1^\mu = \begin{pmatrix} | & | & \cdots & | \\ \mu_1 & \mu_2 & \cdots & \mu_t \\ | & | & & | \end{pmatrix}$ and $\mathcal{L}_2^\mu = \begin{pmatrix} | & | & \cdots & | \\ \nu_1 & \nu_2 & \cdots & \nu_t \\ | & | & & | \end{pmatrix}$.

For each j , f_j and g_j can be extended to \mathbb{C} , by letting f_j and g_j be the identity map outside the image domain Ω . Without loss of generality, we can assume f_j and g_j are normalized quasiconformal maps associated to μ_j and ν_j respectively. If $\alpha > 1$ and $0 < p \leq 1$ satisfy $2 < 2\alpha < 1 + \frac{1}{k}$, then there exist a positive integer $C(k, \alpha)$ such that

$$\|\mathcal{D}_1 f_j - \mathcal{D}_1 g_j\|_2 \leq C(k, \alpha) \|\mu_j - \nu_j\|_q \quad \text{and} \quad \|\mathcal{D}_2 f_j - \mathcal{D}_2 g_j\|_2 \leq C(k, \alpha) \|\mu_j - \nu_j\|_q.$$

where $q = \frac{p\alpha}{\alpha-1}$. Note that all matrix norms are equivalent. There exists a positive constant A such that $\|\cdot\|_q \leq A \|\cdot\|_2$. Hence,

$$\begin{aligned} \|\mathcal{D}\mathbf{f} - \mathcal{D}\mathbf{g}\|_F &= \left(\sum_{j=1}^l \|\mathcal{D}_1 f_j - \mathcal{D}_1 g_j\|_2^2 + \|\mathcal{D}_2 f_j - \mathcal{D}_2 g_j\|_2^2 \right)^{1/2} \\ &\leq \left(\sum_{j=1}^l \frac{2C(k, \alpha)}{A^2} \|\mu_j - \nu_j\|_2^2 \right)^{1/2} \\ &= \sqrt{2}AC(k, \alpha) \|\mathcal{L}_1^\mu - \mathcal{L}_2^\mu\|_F < \sqrt{2}AC(k, \alpha)\epsilon \end{aligned}$$

The second inequality follows by letting $C_1 = \sqrt{2}AC(k, \alpha)$.

For the first inequality, note that f_j and g_j are both normalized quasiconformal map for $j = 1, 2, \dots, l$. Then,

$$f_j = \mathbf{v} + \mathcal{S}\mathcal{D}_2f_j \quad \text{and} \quad g_j = \mathbf{v} + \mathcal{S}\mathcal{D}_2g_j$$

where $\mathbf{v} = \begin{pmatrix} v_1 \\ v_2 \\ \vdots \\ v_n \end{pmatrix} \in \mathbb{C}^n$ is the position vector of all vertices of Ω . $\mathcal{S} \in M_{n \times |F|}(\mathbb{C})$ is defined in such

a way that for any $\mathbf{h} \in \mathbb{C}^{|F|}$, $(\mathcal{S}\mathbf{h})_k = \sum_{m=1}^{|F|} w_{km}(\mathbf{h})_m$, where $w_{km} = \frac{1}{\pi} \int_{T_m} \frac{1}{v_k - \tau} d\tau$ and T_m is the m -th triangular face of Ω . Thus, we have

$$\begin{aligned} \|f_j - g_j\| &= \|\mathcal{S}(\mathcal{D}_2f_j) - \mathcal{S}(\mathcal{D}_2g_j)\|_2 \\ &\leq \|\mathcal{S}\|_2 \|\mathcal{D}_2f_j - \mathcal{D}_2g_j\|_2 \\ &\leq \|\mathcal{S}\|_2 C(k, \alpha) \|\mu_j - \nu_j\|_q. \end{aligned}$$

We can conclude that $\|\mathbf{f} - \mathbf{g}\|_F \leq A\|\mathcal{S}\|_2 C(k, \alpha) \|\mathcal{L}_1^\mu - \mathcal{L}_2^\mu\|_F < A\|\mathcal{S}\|_2 C(k, \alpha)\epsilon$. The first inequality follows by letting $C_1 = A\|\mathcal{S}\|_2 C(k, \alpha)$.

Theorem 4 states that two longitudinal deformations are close if their Beltrami descriptors are close to each others. Furthermore, their degrees of smoothness are similar if their Beltrami descriptors are close. In other words, the longitudinal deformation is stable under the perturbation of the descriptor. It is a crucial observation, so that the manipulation of longitudinal deformations through Beltrami descriptors is not sensitive to the error of the descriptors. On the other hand, to alleviate the issue of large storage requirement, $\mathcal{L}^{\mathcal{F}}$ can be used to replace \mathcal{L}^μ . Theorem 4 tells us the reconstruction error of the longitudinal deformation is small if \mathcal{L}^μ and $\mathcal{L}^{\mathcal{F}}$ are close to each others.

4.3 Decomposition of normal and abnormal components.

In this subsection, we will first explain why the decomposed low-rank and sparse parts would have the meaning as desired and how we can decompose a longitudinal deformation into normal and abnormal components.

To decompose a series of deformations into the normal and abnormal components, we propose to apply the Low-Rank Sparse Matrix Pursuit. Since the normal deformation is defined as the periodic motion displayed on the footage, it should correspond to the low rank part of the matrix capturing the series of deformations. The repeating pattern over a period of duration should be captured by the low rank component. However, when abnormal perturbations occur, the rank will be affected. In particular, the rank of the deformation matrix increases. The abnormal component (or perturbations) should correspond to the sparse part of the deformation matrix. In order to extract the abnormal component from the normal component, decomposing the deformation matrix into low rank and sparse components is a natural strategy.

As a remark, the representation of deformations using the Beltrami descriptor is advantageous. Theoretically, each deformation can be represented by its Beltrami coefficient. Conversely, given a Beltrami coefficient, the associated deformation can be reconstructed by solving the Beltrami's equation. The Beltrami coefficient effectively measures the geometric distortion under the associated deformation. In particular, the associated deformation is guaranteed to be bijective when the magnitude of the Beltrami coefficient is strictly less than 1 everywhere. Thus, representing the deformation matrix using Beltrami coefficients is more robust to the numerical error incurred during the process of low rank and sparse decomposition. On the contrary, if the deformation matrix is represented by vector fields, the bijectivity has to be controlled by the Jacobian constraint, which is hard to enforce. As such, the low rank and sparse decomposition of the deformation matrix represented by vector fields usually yield unnatural deformations with self-overlaps. Nevertheless, the low rank and sparse decomposition of the Beltrami descriptors can effectively decompose the deformations into normal

(periodic) and abnormal (perturbations) motions without self-overlaps, which will be discussed later on.

Given a deformation descriptor \mathcal{L}^μ , we assume \mathcal{L}^μ is composed of the normal deformation \mathcal{N} and abnormal deformation \mathcal{A} . Normal deformation \mathcal{N} is often characterized by repeating pattern. Mathematically, \mathcal{N} can be regarded as periodic and hence it should be of low rank. On the other hand, the abnormal deformation often occurs at some particular region and time. Thus, \mathcal{A} can be assumed to be sparse. As such, our problem can be formulated as finding \mathcal{N} and \mathcal{A} such that they minimize:

$$\min_{\mathcal{N}, \mathcal{A}} \|\mathcal{N}\|_* + \alpha \|\mathcal{A}\|_1, \text{ subject to } \mathcal{L}^\mu = \mathcal{N} + \mathcal{A} \in \mathbb{C}^{mn \times t} \quad (21)$$

The first term involves the nuclear norm, aiming to minimize the rank of \mathcal{N} . The second term aims to enhance the sparsity of \mathcal{A} . The optimization problem can be solved using the alternating minimization method with multiplier (ADMM) as in the real case with suitable modifications. We will describe it in details as follows.

The Augmented Lagrangian function can be written as

$$E(\mathcal{N}^k, \mathcal{A}^k, Z^k; \mathcal{L}^\mu) = \|\mathcal{N}^k\|_* + \alpha \|\mathcal{A}^k\|_1 - \langle Z^k, \mathcal{N}^k + \mathcal{A}^k - \mathcal{L}^\mu \rangle + \frac{\beta_k(N)}{2} \|\mathcal{N}^k + \mathcal{A}^k - \mathcal{L}^\mu\|_2^2 \quad (22)$$

with $\langle X, Y \rangle = \text{real}(\text{tr}(X^*Y)) = \text{real}(\text{tr}(XY^*))$ and $\beta_k(N) = \min \left\{ (1.5)^k \frac{1.25}{\|\mathcal{L}^\mu\|_2}, (1.5)^N \frac{1.25}{\|\mathcal{L}^\mu\|_2} \right\}$. This $\beta_k(N)$ is defined in this way to ensure the recovered abnormal deformation to be bijective. Details will be provided in later section. ADMM to solve the optimization can be written as the following iterative scheme:

$$\begin{cases} \mathcal{N}^{k+1} = \arg \min_{\mathcal{N} \in \mathbb{C}^{mn \times t}} E(\mathcal{N}, \mathcal{A}^k, Z^k; \mathcal{L}^\mu) & (\mathcal{N}\text{-subproblem}) \\ \mathcal{A}^{k+1} = \arg \min_{\mathcal{A} \in \mathbb{C}^{mn \times t}} E(\mathcal{N}^{k+1}, \mathcal{A}, Z^k; \mathcal{L}^\mu) & (\mathcal{A}\text{-subproblem}) \\ Z^{k+1} = Z^k - \beta_k(N)(\mathcal{N}^{k+1} + \mathcal{A}^{k+1} - \mathcal{L}^\mu) \end{cases} \quad (23)$$

We will now describe how each subproblems can be tackled. We begin by looking into the \mathcal{A} -subproblem. Some definitions are needed to help our explanation.

Definition 2 For $A \in \mathbb{C}^{M \times N}$, define the norm

$$\|A\|_{1,2} = \sum_{i=1}^M \left(\sum_{j=1}^N |a_{ij}|^2 \right)^{\frac{1}{2}} \quad (24)$$

It can be easily seen that Equation (24) sums each row's L^2 norm, and it clearly defines a matrix norm as well. Now, the \mathcal{A} -subproblem can be solved via a modified Euclidean projection, as described in the following proposition.

Lemma 1 Define $f : \mathbb{R}^{N \times 2} \rightarrow \mathbb{R}$ by

$$f(X) = \alpha \|X\|_{1,2} + \frac{1}{2} \|M - X\|_2^2 \quad (25)$$

where M is a matrix in $\mathbb{R}^{N \times 2}$. Then the minimiser X^* of f is given by

$$X_j^* = \left(1 - \frac{\alpha}{|M_j|} \right)_+ M_j \quad (26)$$

where X_j^* is the j -th row of X^* and M_j is the j -th row of M . $|M_j|$ is the usual L_2 vector norm and $(y)_+ = \max\{y, 0\}$ for $y \in \mathbb{R}$.

Proof Minimising Equation (25) is equivalent to minimising each row of X . In particular, we must have

$$0 \in \partial \left(\alpha \|X_j^*\|_2 + \frac{1}{2} \|M_j - X_j^*\|_2^2 \right) \quad \text{for } j = 1, 2, \dots, N. \quad (27)$$

For $\|X_j^*\|_2 \neq 0$, we have

$$X_j^* = M_j - \hat{P}_{\mathbb{D}_\infty^\alpha}(M_j) \quad (28)$$

Equation (28) indicates that X_j^* is obtained by reducing the magnitude of M_j by α while keeping the same direction. If $\|M_j^*\|_2 = 0$, then by calculating the subdifferential of Equation (25), we get:

$$0 \in \alpha \{x + \frac{1}{\alpha} M_j \mid x \in \partial(\|X_j^*\|_2)\} \quad (29)$$

Hence, $0 \in \alpha \{g + \frac{1}{\alpha} M_j \mid \|g\|_2 \leq 1\}$. This implies $|M_j| \leq \alpha$. Iterating over each row, we arrive at Equation (26).

Theorem 5 For $\mathcal{N}, \mathcal{A}, Z, \mathcal{L}^\mu \in \mathbb{C}^{(mn) \times t}$, the solution to the \mathcal{A} -subproblem is

$$\mathcal{A}^{k+1} = \frac{1}{\beta_k(N)} Z^k - \mathcal{N}^k + \mathcal{L}^\mu - \hat{P}_{\mathbb{D}_\infty^{\alpha/\beta_k(N)}} \left(\frac{1}{\beta} Z^k - \mathcal{N}^k + \mathcal{L}^\mu \right) \quad (30)$$

where $\hat{P}_{\mathbb{D}_\infty^{\alpha/\beta_k(N)}}$ denotes the Euclidean projection onto $\mathbb{D}_\infty^{\alpha/\beta_k(N)} := \{z \in \mathbb{C} \mid |z| \leq \alpha/\beta_k(N)\}$.

Proof To find the minimizer for the \mathcal{A} -subproblem, it is equivalent to solving

$$\mathcal{A}^{k+1} = \arg \min_{\mathcal{A}} \alpha \|\mathcal{A}\|_1 + \frac{\beta_k(N)}{2} \|\mathcal{N}^k + \mathcal{A} - \mathcal{L}^\mu - \frac{1}{\beta_k(N)} Z^k\|_2^2 \quad (31)$$

Let $\varphi : \mathbb{C}^{(mn) \times t} \rightarrow \mathbb{R}^{(mnt) \times 2}$ be the transformation defined by:

$$\varphi(X) = (\text{Re}(\text{vec}(X)), \text{Im}(\text{vec}(X))) \quad (32)$$

where $\text{vec} : \mathbb{C}^{p \times q} \rightarrow \mathbb{C}^{pq}$ is the function stacking columns of the input matrix into one vector. According to [24], Equation (31) is indeed equivalent to

$$\mathcal{A}^* = \arg \min_{\mathcal{A}} \frac{\alpha}{\beta_k(N)} \|\varphi(\mathcal{A})\|_{1,2} + \frac{1}{2} \|\varphi(\mathcal{N}^k) + \varphi(\mathcal{A}) - \varphi(\mathcal{L}^\mu) - \frac{1}{\beta_k(N)} \varphi(Z^k)\|_F^2 \quad (33)$$

where $\|X\|_{1,2} = \sum_{j=1}^n \|X_j\|_2$ with X_j denotes the j -th row of X .

Putting $M = \frac{1}{\beta_k(N)} Z^k - \mathcal{N}^k + \mathcal{L}^\mu$, according to Lemma 1, it follows that with \mathcal{A}_j^* and M_j denoting the j -th row of \mathcal{A} and M respectively,

$$\mathcal{A}_j^* = \left(1 - \frac{\alpha}{\beta_k(N)} \frac{1}{|M_j|} \right)_+ M_j \quad (34)$$

If $|M_j| \leq \frac{\alpha}{\beta_k(N)}$, $\mathcal{A}_j^* = 0$. If $|M_j| > \frac{\alpha}{\beta_k(N)}$,

$$\begin{aligned} \mathcal{A}_j^* &= \left(1 - \frac{\alpha}{\beta_k(N)} \frac{1}{|M_j|} \right) M_j \\ &= M_j - \hat{P}_{\mathbb{D}_\infty^{\alpha/\beta_k(N)}}(M_j) \end{aligned} \quad (35)$$

Then Formula (30) follows.

Theorem (31) is important as it gives us a closed form solution to solve the \mathcal{A} -subproblem during the ADMM iteration.

Next, we will look at the \mathcal{N} -subproblem. Indeed, the \mathcal{N} -subproblem can be treated exactly as in the real case, which is described as follows.

Theorem 6 For $\mathcal{N}, \mathcal{A}, Z, \mathcal{L}^\mu \in \mathbb{C}^{mn \times t}$, the solution to the low-rank subproblem in Equation (10) is

$$\mathcal{N}^{k+1} = U^{k+1} \text{diag} \left(\max\{\sigma_i^{k+1} - \frac{1}{\beta_k(N)}, 0\} \right) (V^{k+1})^T \quad (36)$$

where $U^{k+1}, V^{k+1}, \sigma_i^{k+1}$ are obtained by SVD that is:

$$\mathcal{L}^\mu - \mathcal{A}^{k+1} + \frac{1}{\beta_k(N)} Z^k = U^{k+1} \Sigma^{k+1} (V^{k+1})^T \quad \text{with} \quad \Sigma^{k+1} = \text{diag}(\{\sigma_i^{k+1}\}_{i=1}^r) \quad (37)$$

The proof of the above theorem follows similarly as in the case of real-valued matrices. We refer readers to [40, 2] for the details of the proof.

It is worth mentioning that different literature has provided theoretical guarantee that the ADMM approach on this RPCA will converge. Readers can refer to [20, 54, 13, 12, 16, 17, 18, 53]. In particular, Hong et. al. [20] proved that the approach has linear time convergence.

We summarize the algorithm for the decomposition of \mathcal{L}^μ into normal and abnormal deformations as follows.

Algorithm 1: Decomposition of \mathcal{L}^μ

Input : $\mathcal{L}^\mu \in \mathbb{C}^{mn \times t}$, $N \in \mathbb{N}$
Output : Normal component \mathcal{N} and abnormal component \mathcal{A}
Initialisation: \mathcal{N}_0 be a zero matrix, $Z_0 = \mathcal{L}^\mu / \|\mathcal{L}^\mu\|_2$,
 $\beta_k(N) = \min\{(1.5)^k \frac{1.25}{\|\mathcal{L}^\mu\|_2}, (1.5)^N \frac{1.25}{\|\mathcal{L}^\mu\|_2}\}$
while not converge **do**
 Update \mathcal{N}^{k+1} using Equation (36) ;
 Update \mathcal{A}^{k+1} using Equation (30) ;
 $Z_{k+1} \leftarrow Z_k + \beta_k(n)(\mathcal{L}^\mu - \mathcal{N}^{k+1} - \mathcal{A}^{k+1})$
end

Here, N is a chosen integer parameter. Once \mathcal{L}^μ is decomposed into \mathcal{N} and \mathcal{A} , the associated normal and abnormal longitudinal deformations can be reconstructed according to Equation (19).

The subtle perturbation from a longitudinal deformation are supposedly bijective without overlaps. A crucial question is whether our extracted abnormal deformation is indeed bijective. As a matter of fact, performing the low rank and sparse decomposition on the Beltrami descriptor is beneficial, since we can theoretically guarantee the bijectivity of the extracted abnormal deformation under suitable choice of the parameter. Hence, our algorithm can give a realistic and accurate extracted component for further deformation analysis. This fact is explained in details with the following theorem.

Theorem 7 Considering Equation (22), there exists a constant $c(\mathcal{L}^\mu)$ such that if

$$\alpha > c(\mathcal{L}^\mu) = \frac{\|\mathcal{L}^\mu\|_{\max}}{\|\mathcal{L}^\mu\|_2} + \frac{1.25p}{\|\mathcal{L}^\mu\|_2} \frac{1 - (1.5)^N q^N}{1 - 1.5q} + \frac{\beta_N(N)pq^N}{1 - q} \quad (38)$$

where p, q depend on \mathcal{L}^μ and $\|\mathcal{L}^\mu\|_{\max} < 1$, then our algorithm 1 would yield $\|\mathcal{A}^k\|_{\max} < 1$ for all $k \in \mathbb{N}$.

Proof The proof is based on induction on k . We first check the base case

$$\begin{aligned} \|\mathcal{A}^1\|_{\max} &= \left\| \frac{1}{\beta_0} Z^0 + \mathcal{L}^\mu - \hat{P}_{\mathbb{D}_\infty^{\alpha/\beta_0}} \left(\frac{1}{\beta_0} Z^0 + \mathcal{L}^\mu \right) \right\|_{\max} < 1 \\ \iff \left\| \frac{1}{\beta_0} Z^0 + \mathcal{L}^\mu \right\|_{\max} &< 1 + \frac{\alpha}{\beta_0} \end{aligned} \quad (39)$$

Clearly, $\|\mathcal{L}^\mu\|_{\max} < 1$ and since Z^0 is defined to be $\mathcal{L}^\mu/\|\mathcal{L}^\mu\|_2$, we proved the base case.

Assume it is true that $\|\mathcal{A}^k\|_{\max} < 1$. From [20] by Hong et. al., we have, for some constant $p > 0$, $q \in (0, 1)$

$$\|\mathcal{L}^\mu - \mathcal{N}^r - \mathcal{A}^r\| \leq pq^r \quad (40)$$

which is known as the R-linearity of convergence of ADMM. Note that using Equation (30) in Formula (39)

$$\|\mathcal{A}^{k+1}\|_{\max} < 1 \iff \left\| \frac{1}{\beta_k(N)} Z^k - \mathcal{N}^k + \mathcal{L}^\mu \right\|_{\max} < 1 + \frac{\alpha}{\beta_k(N)} \quad (41)$$

Considering this specific term, we deduce that

$$\begin{aligned} & \left\| \frac{1}{\beta_k(N)} Z^k - \mathcal{N}^k + \mathcal{L}^\mu \right\|_{\max} \\ &= \left\| \frac{1}{\beta_k(N)} \left(\frac{\mathcal{L}^\mu}{\|\mathcal{L}\|_2} + \sum_{i=1}^{k-1} \beta_i(N) (\mathcal{L}^\mu - \mathcal{N}^i - \mathcal{A}^i) \right) - \frac{\beta_k(N)}{\beta_k(N)} (\mathcal{L}^\mu - \mathcal{N}^k - \mathcal{A}^i) + \mathcal{A}^k \right\|_{\max} \\ &\leq \frac{1}{\beta_k(N)} \left\| \frac{\mathcal{L}^\mu}{\|\mathcal{L}\|_2} + \sum_{i=1}^k \beta_i(N) (\mathcal{L}^\mu - \mathcal{N}^i - \mathcal{A}^i) \right\|_{\max} + \|\mathcal{A}^k\|_{\max} \end{aligned} \quad (42)$$

Notice that using Equation (40), we have

$$\begin{aligned} & \left\| \frac{\mathcal{L}^\mu}{\|\mathcal{L}\|_2} + \sum_{i=1}^k \beta_i(N) (\mathcal{L}^\mu - \mathcal{N}^i - \mathcal{A}^i) \right\|_{\max} \\ &= \frac{\|\mathcal{L}^\mu\|_{\max}}{\|\mathcal{L}^\mu\|_2} + \sum_{i=1}^{n-1} \beta_i(N) \|\mathcal{L}^\mu - \mathcal{N}^i - \mathcal{A}^i\|_{\max} + \sum_{i=n}^k \beta_i(N) \|\mathcal{L}^\mu - \mathcal{N}^i - \mathcal{A}^i\|_{\max} \\ &\leq \frac{\|\mathcal{L}^\mu\|_{\max}}{\|\mathcal{L}^\mu\|_2} + \sum_{i=1}^{n-1} \beta_i(N) pq^i + \sum_{i=n}^k \beta_i(N) pq^i \\ &= \frac{\|\mathcal{L}^\mu\|_{\max}}{\|\mathcal{L}^\mu\|_2} + \frac{1.25p}{\|\mathcal{L}^\mu\|_2} \frac{1 - (1.5)^N q^N}{1 - 1.5q} + \frac{\beta_N(N) pq^N}{1 - q} \\ &< \alpha \end{aligned} \quad (43)$$

Thus, putting the last Inequality (43) into Equation (42), we have

$$\left\| \frac{1}{\beta_k(N)} Z^k - \mathcal{N}^k + \mathcal{L}^\mu \right\|_{\max} < \frac{\alpha}{\beta_k(N)} + 1 \quad (44)$$

which implies that $\|\mathcal{A}^{k+1}\|_{\max} < 1$, which completes the inductive proof.

With all tools introduced, we can now describe our whole algorithm as follows.

Algorithm 2: Abnormal Deformation Extraction and Recovery Algorithm

Input : Reference frame I_{ref} , and video frame $\{I_i\}_{i=1}^t$
Output: Low-rank frames $\{\mathbf{l}_i\}_{i=1}^t$ and sparse frames $\{\mathbf{s}_i\}_{i=1}^t$
for each frame I_i (*parallel-computation compatible*) **do**
 | Register I_{ref} to I_i get the deformation field;
 | Compute the Beltrami descriptor \mathcal{L}^μ ;
end
Using algorithm 1, decompose $\mathcal{L}^\mu = \mathcal{N} + \mathcal{A}$;
for each column l_i of \mathcal{N} (*parallel-computation compatible*) **do**
 | Using LBS, recover l_i to a map $f_i^{\mathcal{N}}$;
 | Deform I_{ref} with the map $f_i^{\mathcal{N}}$ and we obtain \mathbf{l}_i ;
end
for each column s_i of \mathcal{A} (*parallel-computation compatible*) **do**
 | Using LBS, recover s_i to a map $f_i^{\mathcal{A}}$;
 | Deform I_{ref} with the map $f_i^{\mathcal{A}}$ and we obtain \mathbf{s}_i ;
end

Finally, we remark that the robustness actually depends on the accuracy of the registration. For a large deformation between the reference frame and the image frame, some registration methods may not yield accurate registration result. As a result, the decomposition of the series of deformations may become inaccurate. Nevertheless, if the deformation across all frames are not very large, we can achieve similar performance whichever frame is chosen as the reference frame. For the case with large deformations across frames, we usually choose a frame, which is least deviated from every frame, as the reference image. With this choice, our method can still achieve very accurate decomposition effectively.

5 Experimental Result

In this section, we present our experimental results on synthetic images, as well as on real medical images.

Example 1: We first test our proposed method on a synthetic image sequence. The input data is a sequence of binary images that shows a circle shrinks and expands, and repeats this process for a few cycles. Readers can refer to Figure 2 to visualise this process. The total number of frame of this process is 48, which means that the ground-truth rank of the Fourier Transformed BC matrix is 24. The whole expansion and contraction process is repeated 9 times, and 3 of which are perturbed

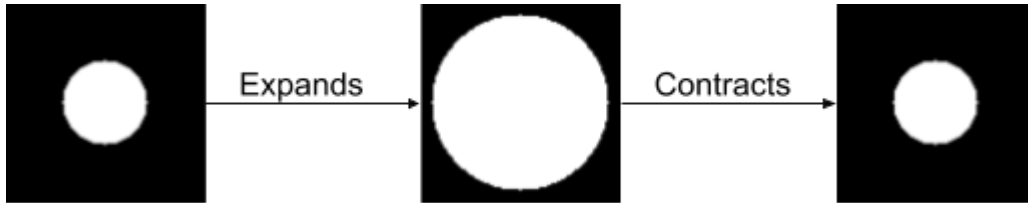


Fig. 2: Illustration of a Normal Cycle of the First Synthetic Experiment

by adding some deformations around the boundary of the circle. After adding perturbation on the cycles, the rank of the Beltrami descriptor matrix raises to 47, while our algorithm successfully reduces the rank of the low-rank matrix to 27. We remark that since we took the smallest circle as the reference image, one can observe that the recovered sparse image has a circle that is far smaller than perturbed frames. Table 1 shows the result of our algorithm on one of the three perturbations.

| Original Frame | Perturbed Frame | Recovered Low-Rank Frame | Recovered Sparse Frame | Recovered Low-Rank Frame on Vector Field | Recovered Sparse Frame on Vector Field |
|----------------|-----------------|--------------------------|------------------------|--|--|
| | | | | | |
| | | | | | |
| | | | | | |
| | | | | | |
| | | | | | |
| | | | | | |
| | | | | | |

Table 1: Results of Example 1

A straightforward method to decompose the longitudinal deformation is done by applying the RPCA method on the vector fields of the deformation. As mentioned, vector fields cannot effectively capture the geometric information of the deformation. As such, RPCA method on vector fields cannot yield satisfactory results. The last two columns of Table 1 show the results of pursuing the low-rank and sparse part on the deformation vector fields obtained from registering the reference frame to each of the video frames. We view each vector in the vector fields as an element in \mathbb{C} , and we stacked them horizontally and obtain a giant matrix, with each column corresponds to the deformation vector field from the referenced frame to each frame defined at each pixel. Then we run the complex matrix decomposition algorithm on this matrix. Although the decomposed low-rank matrix is of rank 24, the last two columns of Table 1 clearly shows that the recovered results are far from the ground-truth to be useful: The circles are distorted to ellipses, which they should not be. Compared to the results obtained from our original longitudinal deformation descriptor, this decomposition is not meaningful.

Example 2: The next example is on a sequence of real medical images of a beating heart. The original video contains 341 frames with repeated periodic beating of 31 times. In this example, artificial abnormal deformations are introduced to one of the 31 cycles, and so ground-truth images

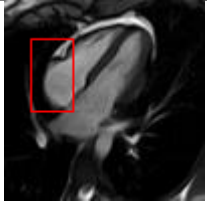
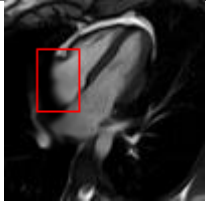
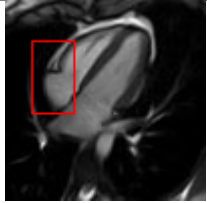
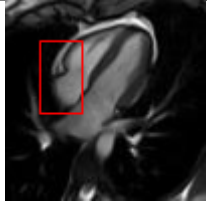
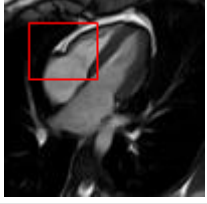
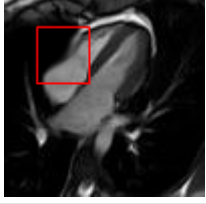
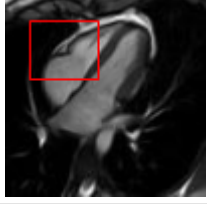
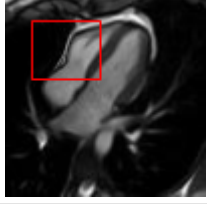
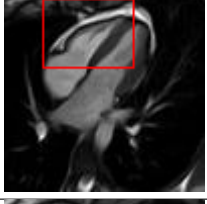

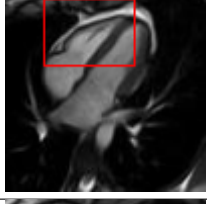





| Original Frame | Perturbed Frame | Recovered Low-Rank Frame | Recovered Sparse Frame |
|--|--|--|--|
|  |  |  |  |
|  |  |  |  |
|  |  |  |  |
|  |  |  |  |

Table 2: Results of Example 2

are available to study the accuracy of our proposed model. Table 2 shows the result. The second column shows the frames with manual deformation added on images in the first column, and the red box area is where deformation is added. We can see that our algorithm can almost recover the low-rank frames to the original frames and the sparse frames to the perturbed frames. The size of the input Beltrami descriptor is 19602×341 , and the rank of the original video and perturbed video are 11 and 15 respectively. After running our algorithm on the matrix, the rank of the recovered low-rank matrix is reduced to 11.

Beside the recovered rank, from Table 2, we can see that our algorithm can capture and recover both the normal and abnormal deformation on the beating heart to great details. It can be seen that the recovered low-rank frames looks very much alike to the original frames and recovered sparse frames can effective capture the abnormal deformation.

To better observe the result of our experiment, Figure 3 shows the second row of Table 2. The area bounded by the red box is the periphery of the beating heart. Figure 3(a) shows the ground truth frame. Figure 3(b) shows a frame with a perturbation combined with the normal deformation. The deformation between a frame and the reference image is computed by registration and represented by the Beltrami coefficient. Figure 3(c) shows the deformed image from the reference frame by the low rank part of the deformation. It closely resemble the ground truth frame as shown in Figure 3(a). Figure 3(d) shows the deformed image from the reference frame by the sparse part of the deformation. It demonstrates how the abnormal motion deforms the image from the reference frame. Thus, Figure 3(d) should be different from Figure 3(b), since Figure 3(b) combines both the normal and abnormal motions.

Figure 4 shows the visualisation of Figure 3 mappings in the form of grids. Let μ_1 and μ_2 be the Beltrami coefficients of the registration maps from the reference frame to the ground truth frame

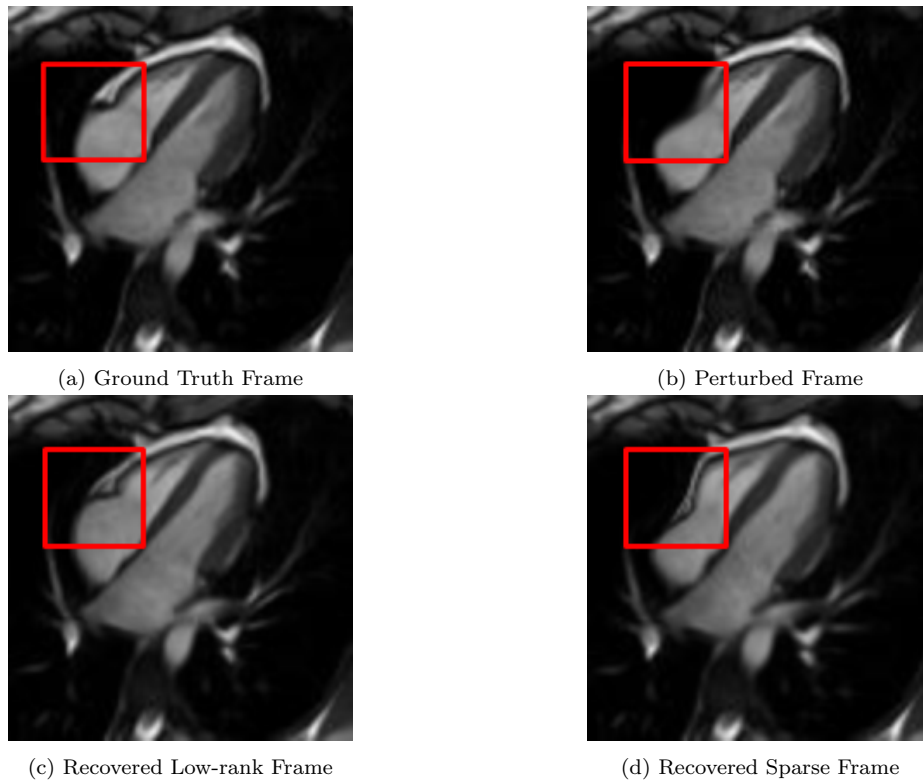


Fig. 3: Second Row of Table 2

in Figure 3(a) and the perturbed frame in Figure 3(b) respectively. Figure 4(a) shows the mapping associated to Beltrami coefficient μ_1 , and Fig 4(b) shows the mapping associated to BC $\mu_2 - \mu_1$. From Figure 4(c) and Fig 4(d), we can see that our method successfully restored the normal and abnormal deformation. Figure 4 serves as evidence that our decomposition is meaningful, in the sense that our method does not blindly return a Beltrami Descriptor with certain periodicity, but the decomposed descriptor does carry our desired information to recover the deformation to a large extent.

Example 3: In this example, we test our algorithm on another medical video of a beating heart with abnormal perturbations. The original rank of the video is 36. After performing our proposed method on the Beltrami descriptor, the rank of the low-rank matrix is reduced to 20. Table 3 displays one of the perturbation and its recovery by our method. As shown in the table, the results show that our algorithm can recover the normal and abnormal deformation. Readers can compare the first column with the third, and the second with the fourth.

Figure 5 shows the ground truth and recovered maps of the registration maps in the last row of Table 4. It can be seen that ground truth low-rank mapping shown in Figure 5(a) resembles the recovered low-rank mapping shown in Figure 5(c). This again shows that we could obtain a meaningful mapping from the decomposition.

Example 4: In this example, we test our algorithm on another medical video of a lung under respiration. The original video capture 31 cycles with some perturbation at some frames. The rank of the input longitudinal Beltrami descriptor is 23, which was reduced to 10 after performing our algorithm on it. Table 4 showed the pictures of one of the perturbation.

In addition to running this experiment on our algorithm, we again test decomposing the vector field matrix as in Example 1. We stacked the registration deformation vector fields from the reference image to all other frames in the video into one giant matrix over complex field. Then, running the complex low-rank and sparse component pursuit on the matrix gave the last two columns in Table 4. It is clear that the decomposed sparse matrix can barely capture any abnormal deformation as

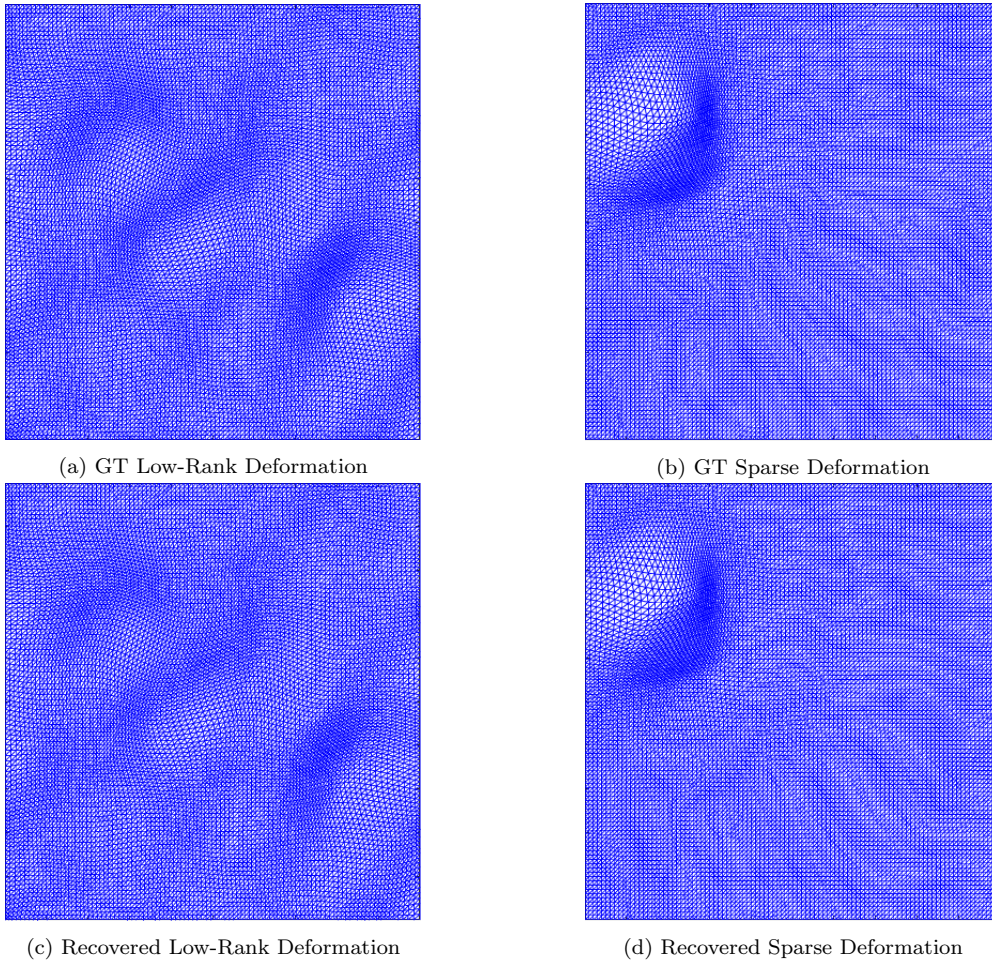


Fig. 4: Comparison Between Ground-Truth Maps and Recovered Maps

does the Beltrami descriptor. Our experiment once again shows that applying the algorithm to decompose on vector field matrices is not the best choice.

Figure 6 displays the 4 mappings as in Example 3 and 4. Again, we can see that after the decomposition of the Beltrami descriptor, the decomposed mappings to large extent resemble the corresponding ones.

Example 5: In this example, we test our proposed method on another medical video of a breathing lung with abnormal perturbation. The original video captures 36 cycles. The rank of the Beltrami descriptor matrix is 26. Our proposed method recovers the low rank matrix with rank 12. Table 5 displays the results of one of the perturbation using our algorithm. Again, our proposed method effectively decompose the longitudinal deformation into the normal periodic component and abnormal component.

Finally, we summarize the rank of the decomposed sparse component for each example in Table 6. The ranks of the original input Beltrami descriptors are also recorded. Note that our proposed algorithm can effectively obtain the sparse component that reduces the rank. The rank of the sparse component closely resemble to the rank of the Beltrami descriptor of the video without abnormal perturbations.

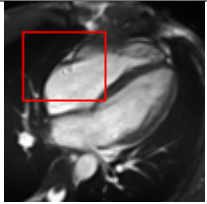
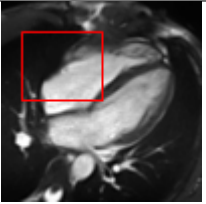
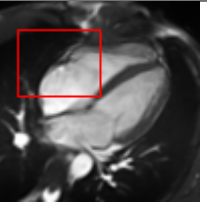
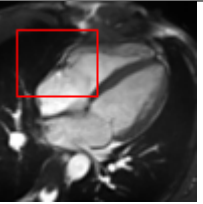
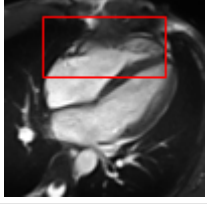
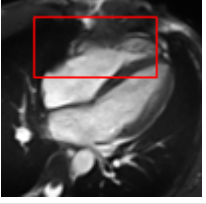
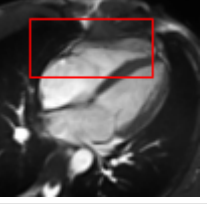
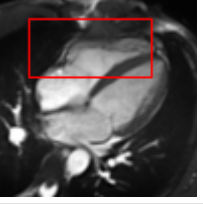
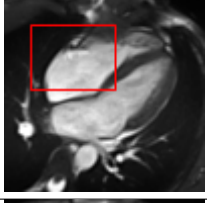
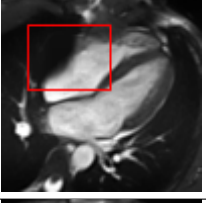
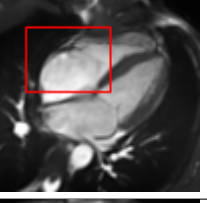
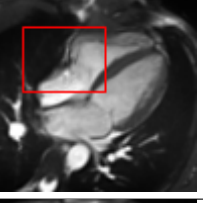
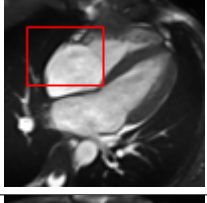
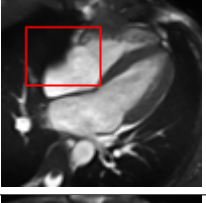
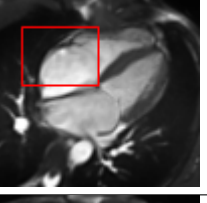
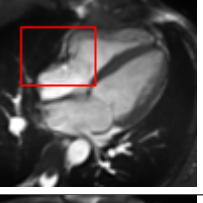
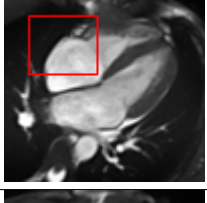
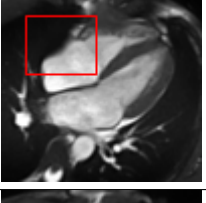
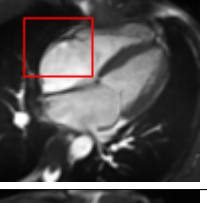
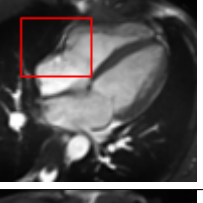
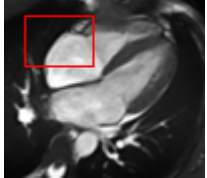
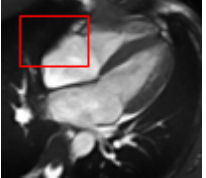
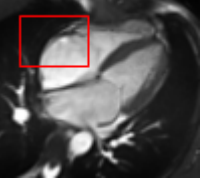
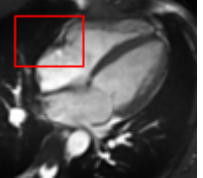
| Frame without abnormal deformation | Frame with abnormal deformation | Recovered Low-Rank Frame | Recovered Sparse Frame |
|---|---|---|---|
|  |  |  |  |
|  |  |  |  |
|  |  |  |  |
|  |  |  |  |
|  |  |  |  |
|  |  |  |  |

Table 3: Result of Example 3

6 Conclusion and future works

We address the problem of decomposing a longitudinal deformation into the normal periodic component and the abnormal irregular component. Our strategy is to represent the longitudinal deformation by the proposed Beltrami descriptor and apply RPCA on it. The low rank part effectively extracts the normal component, while the sparse part effectively captures the irregular deformation. The Beltrami descriptor describes the geometric information about the deformation, and hence performing the decomposition on the Beltrami descriptor yields meaningful results. In particular, we can prove that the extracted abnormal motion is guaranteed to be bijective under suitable choice of parameters. Extensive experiments on both synthetic and real data give encouraging results.

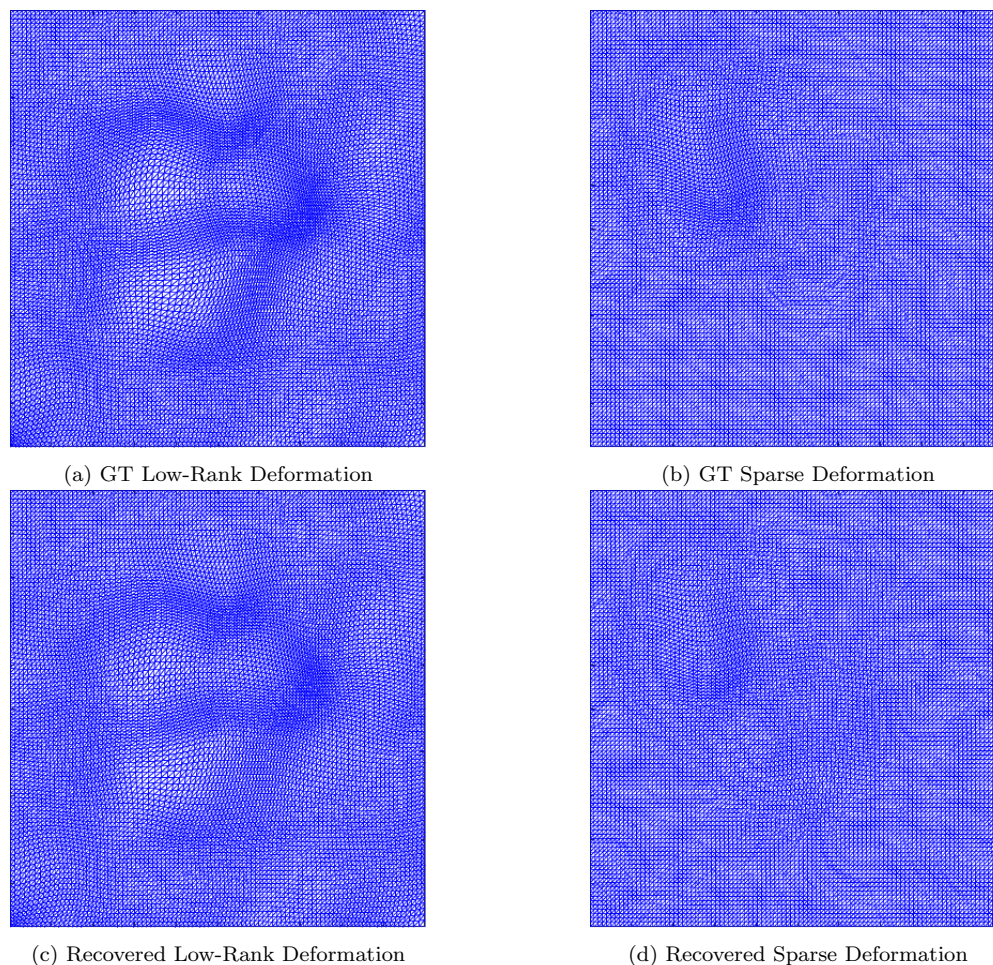


Fig. 5: Comparison Between Ground-Truth Maps and Recovered Maps

In this paper, we applied Low-Rank Sparse Matrix Pursuit to videos that are subject to periodic motion. We conjectured that this method, with some variations, can also be applied to videos subject to some constant deformations. For example, we might want to segment out a walking pedestrian with vehicles moving from left to right in the background. We hypothesized that the Beltrami descriptor could also be obtained using some registration techniques, such as the optical flow method. The descriptor of the moving background again should be of low-rank, and the pedestrian should be described by the sparse descriptor. This is our potential continuation of this project.

References

1. Beg, M.F., Miller, M., Trounev, A., Younes, L.: Computing large deformation metric mappings via geodesic flows of diffeomorphisms. *International Journal of Computer Vision* **61**, 139–157 (2005). DOI 10.1023/B:VISI.0000043755.93987.aa
2. Cai, J.F., Candès, E.J., Shen, Z.: A singular value thresholding algorithm for matrix completion (2008)
3. Candès, E.J., Li, X., Ma, Y., Wright, J.: Robust principal component analysis? *Journal of ACM* **58** (3) (2011). URL <https://doi.org/10.1145/1970392.1970395>
4. Cao, W., Wang, Y., Sun, J., Meng, D., Yang, C., Cichocki, A., Xu, Z.: Total variation regularized tensor rpca for background subtraction from compressive measurements. *IEEE Transactions on Image Processing* **25**(9), 4075–4090 (2016). DOI 10.1109/TIP.2016.2579262
5. Chan, H., Li, L., Lui, L.: Quasi-conformal statistical shape analysis of hippocampal surfaces for Alzheimer’s disease analysis. *Journal of Neurocomputing* **175**(A), 177–187 (2016)
6. Chan, H.L., Yan, S., Lui, L.M., Tai, X.C.: Topology-preserving image segmentation by beltrami representation of shapes. *Journal of Mathematical Imaging and Vision* **60**(3), 401–421 (2018)

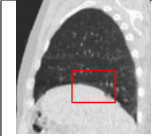
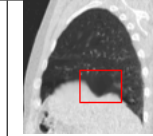
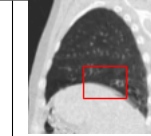
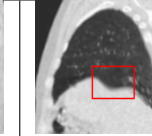
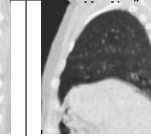
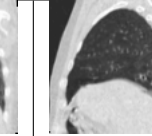
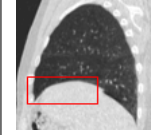
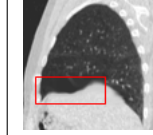
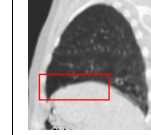
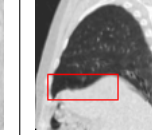
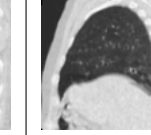
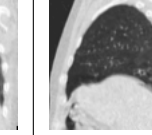

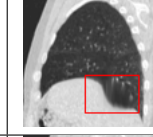
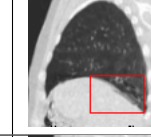
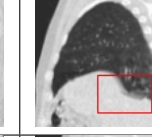
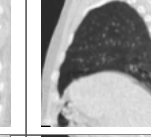
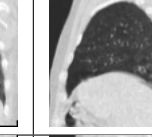
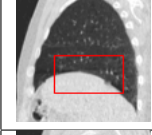
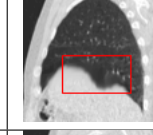
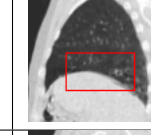
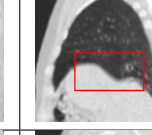
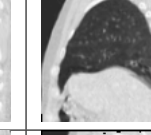
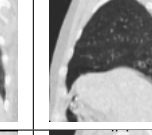
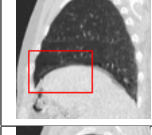
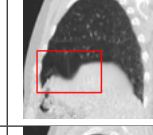

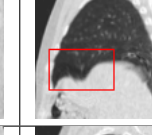
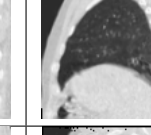
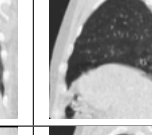
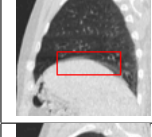
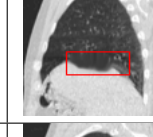
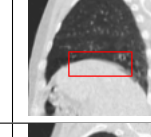
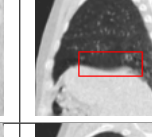
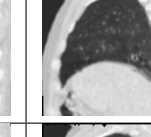
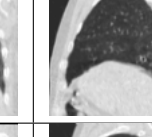
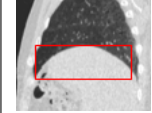
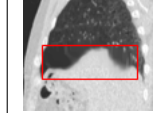
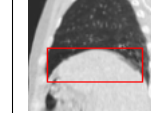
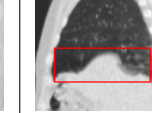
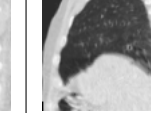
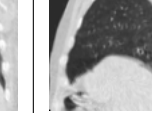
| Original Frame | Perturbed Frame | Recovered Low-Rank Frame | Recovered Sparse Frame | Recovered Sparse Frame on Vector Field with FFT | Recovered Sparse Frame on Vector Field without FFT |
|---|---|---|---|--|---|
|  |  |  |  |  |  |
|  |  |  |  |  |  |
|  |  |  |  |  |  |
|  |  |  |  |  |  |
|  |  |  |  |  |  |
|  |  |  |  |  |  |
|  |  |  |  |  |  |

Table 4: Result of Example 4

7. Chan, H.L., Yuen, H.M., Au, C.T., Chan, K.C.C., Li, A.M., Lui, L.M.: Quasi-conformal geometry based local deformation analysis of lateral cephalogram for childhood osa classification. arXiv preprint arXiv:2006.11408 (2020)
8. Choi, G.P., Qiu, D., Lui, L.M.: Shape analysis via inconsistent surface registration. *Proceedings of the Royal Society A* **476**(2242), 20200,147 (2020)
9. Choi, P., Chan, H., Yong, R., Ranjitkar, S., Brook, A., Townsend, G., Chen, K., Lui, L.: Tooth morphometry using Quasi-conformal theory. *Pattern Recognition* **99**, 107,064 (2020)
10. Choi, P.T., Lam, K.C., Lui, L.M.: Flash: Fast landmark aligned spherical harmonic parameterization for genus-0 closed brain surfaces. *SIAM Journal on Imaging Sciences* **8**(1), 67–94 (2015)
11. Ebadi, S.E., Izquierdo, E.: Foreground segmentation with tree-structured sparse rpca. *IEEE Transactions on Pattern Analysis and Machine Intelligence* **40**(9), 2273–2280 (2018). DOI 10.1109/TPAMI.2017.2745573
12. Gabay, D.: Chapter ix applications of the method of multipliers to variational inequalities. In: M. Fortin, R. Glowinski (eds.) *Augmented Lagrangian Methods: Applications to the Numerical Solution of Boundary-Value Problems*, *Studies in Mathematics and Its Applications*, vol. 15, pp. 299 – 331. Elsevier (1983). DOI [https://doi.org/10.1016/S0168-2024\(08\)70034-1](https://doi.org/10.1016/S0168-2024(08)70034-1). URL <http://www.sciencedirect.com/science/article/pii/S0168202408700341>
13. Gabay, D., Mercier, B.: A dual algorithm for the solution of nonlinear variational problems via finite element approximation. *Computers & Mathematics with Applications* **2**(1), 17 – 40 (1976). DOI [https://doi.org/10.1016/0898-1221\(76\)90003-1](https://doi.org/10.1016/0898-1221(76)90003-1). URL <http://www.sciencedirect.com/science/article/pii/0898122176900031>

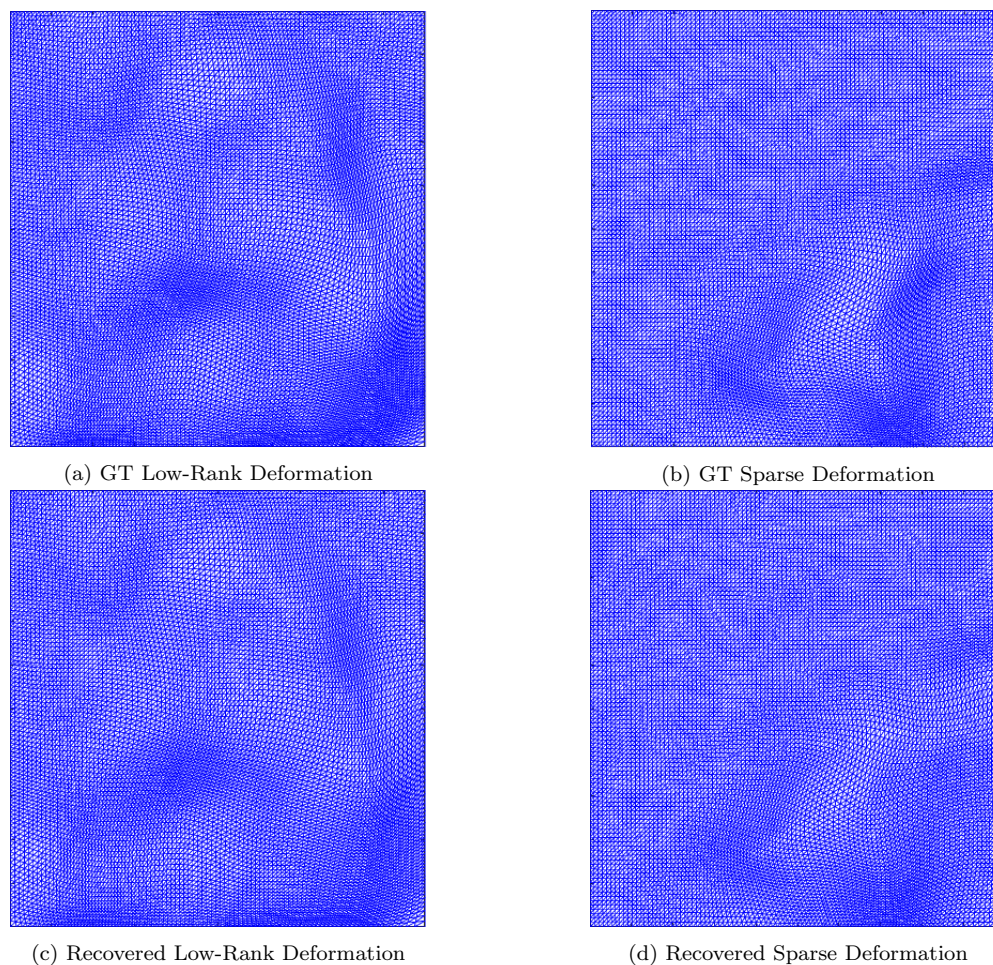


Fig. 6: Comparison Between Ground-Truth Maps and Recovered Maps

14. Gardiner, F., Lakic, N., Society, A.M.: Quasiconformal Teichmüller Theory. Mathematical surveys and monographs. American Mathematical Society (2000). URL <https://books.google.de/books?id=BLfyBwAAQBAJ>
15. Gilmartin JJ, G.G.: Abnormalities of chest wall motion in patients with chronic airflow obstruction. *Thorax* (1984)
16. Glowinski, R.: Numerical Methods for Nonlinear Variational Problems. Scientific Computation. Springer Berlin Heidelberg (2013). URL <https://books.google.co.uk/books?id=vGrwCAAAQBAJ>
17. Glowinski, R., Le Tallec, P.: Augmented Lagrangian and Operator-Splitting Methods in Nonlinear Mechanics. Society for Industrial and Applied Mathematics (1989). DOI 10.1137/1.9781611970838. URL <https://epubs.siam.org/doi/abs/10.1137/1.9781611970838>
18. He, B., Yang, H.: Some convergence properties of a method of multipliers for linearly constrained monotone variational inequalities. *Operations Research Letters* **23**(3), 151 – 161 (1998). DOI [https://doi.org/10.1016/S0167-6377\(98\)00044-3](https://doi.org/10.1016/S0167-6377(98)00044-3). URL <http://www.sciencedirect.com/science/article/pii/S0167637798000443>
19. Heaton J, Y.S.: Premature atrial contractions. StatPearls [Internet]. Treasure Island (FL): StatPearls Publishing (2021). URL <https://www.ncbi.nlm.nih.gov/books/NBK559204/>
20. Hong, M., Luo, Z.Q.: On the linear convergence of the alternating direction method of multipliers (2012)
21. Islam, M., Kabir, M.: A new feature-based image registration algorithm. *Computer Technology and Application* **4**, 79–84 (2013)
22. Javed, S., Oh, S.H., Sobral, A., Bouwmans, T., Jung, S.K.: Background subtraction via superpixel-based on-line matrix decomposition with structured foreground constraints. In: 2015 IEEE International Conference on Computer Vision Workshop (ICCVW), pp. 930–938 (2015). DOI 10.1109/ICCVW.2015.123
23. Kaplan, J., Donoho, D.: The morphlet transform: A multiscale representation for diffeomorphisms. *Proceedings of the Workshop on Image Registration in Deformable Environments* pp. 21–30 (2006)
24. Kumar, A., Chan, T.: Iris recognition using quaternionic sparse orientation code (qsoc). In: 2012 IEEE Computer Society Conference on Computer Vision and Pattern Recognition Workshops, pp. 59–64 (2012). DOI 10.1109/CVPRW.2012.6239216
25. Lam, K., Ng, T., Lui, L.: Multiscale representation of deformation via Beltrami coefficients. *SIAM Journal of Multiscale Modeling and Simulation* **15**(2), 864–891 (2017)

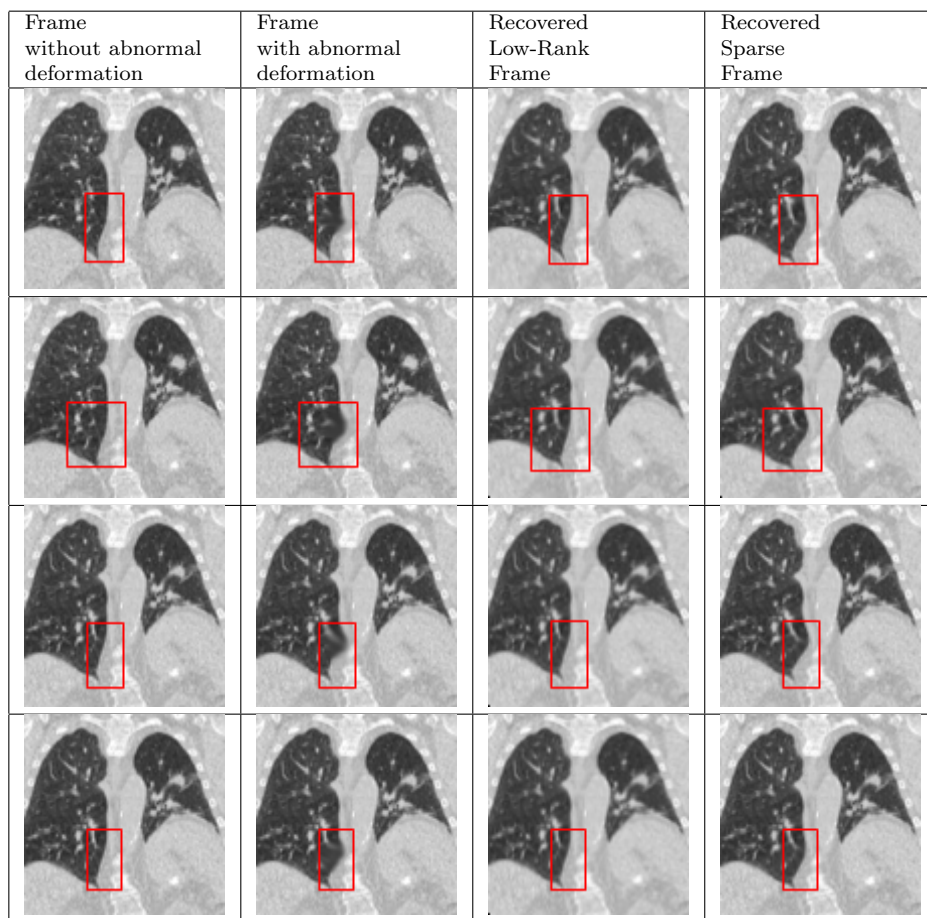


Table 5: Result of Example 5

| | size of input matrix | rank of input matrix without perturbation | rank of input matrix with perturbation | rank of recovered low-rank matrix | Decomposition Time (s) |
|--------------------------|----------------------|---|--|-----------------------------------|------------------------|
| Synthetic Circle Example | 19602×431 | 24 | 47 | 27 | 167.06 |
| First Heart Example | 19602×341 | 11 | 15 | 11 | 44.80 |
| Second Heart Example | 19602×378 | 18 | 36 | 20 | 98.41 |
| First Lung Example | 19602×310 | 10 | 23 | 10 | 21.98 |
| Second Lung Example | 19602×360 | 10 | 26 | 12 | 79.96 |

Table 6: Summary of Recovered Rank by Our Proposed Algorithm

26. Lam, K.C., Lui, L.M.: Landmark- and Intensity-based registration with large deformations via Quasi-conformal maps. *SIAM Journal on Imaging Sciences* **7**(4), 2364–2392 (2014). DOI 10.1137/130943406. URL <https://doi.org/10.1137/130943406>
27. Lee, Y.T., Lam, K.C., Lui, L.M.: Landmark-matching transformation with large deformation via n-dimensional quasi-conformal maps. *Journal of Scientific Computing* **67**(3), 926–954 (2016)
28. Lehto, O., Virtanen, K.: Quasiconformal mappings in the plane (2011)
29. Li, Y., Liu, G., Liu, Q., Sun, Y., Chen, S.: Moving object detection via segmentation and saliency constrained rpca. *Neurocomputing* **323**, 352 – 362 (2019). DOI <https://doi.org/10.1016/j.neucom.2018.10.012>. URL <http://www.sciencedirect.com/science/article/pii/S0925231218311883>
30. Lin, Z., Chen, M., Ma, Y.: The augmented lagrange multiplier method for exact recovery of corrupted low-rank matrices. *Mathematical Programming* **9** (2010)
31. Lin, Z., Ganesh, A., Wright, J., Wu, L., Chen, M., Ma, Y.: Fast convex optimization algorithms for exact recovery of a corrupted low-rank matrix. In: *Intl. Workshop on Comp. Adv. in Multi-Sensor Adapt. Processing*, Aruba,

- Dutch Antilles (2009)
32. Lui, L., Wong, T., Gu, X., Thompson, P., Chan, T., Yau, S.: Shape-based diffeomorphic registration on hippocampal surfaces using Beltrami holomorphic flow. *Medical Image Computing and Computer Assisted Intervention (MICCAI)*, art II, LNCS 6362 pp. 323–330 (2010)
 33. Lui, L., Wong, T., Zeng, W., Gu, X., Thompson, P., Chan, T., Yau, S.: Detection of shape deformities using Yamabe flow and Beltrami coefficients. *Journal of Inverse Problem and Imaging (IPI)* **4**(2), 311–333 (2010)
 34. Lui, L.M., Lam, K.C., Wong, T.W., Gu, X.: Texture map and video compression using Beltrami representation. *SIAM Journal on Imaging Sciences* **6**(4), 1880–1902 (2013)
 35. Lui, L.M., Lam, K.C., Yau, S.T., Gu, X.: Teichmüller mapping (t-map) and its applications to landmark matching registration. *SIAM Journal on Imaging Sciences* **7**(1), 391–426 (2014)
 36. Lui, L.M., Thiruvenkadam, S., Wang, Y., Thompson, P.M., Chan, T.F.: Optimized conformal surface registration with shape-based landmark matching. *SIAM Journal on Imaging Sciences* **3**(1), 52–78 (2010)
 37. Lui, L.M., Wen, C.: Geometric registration of high-genus surfaces. *SIAM Journal on Imaging Sciences* **7**(1), 337–365 (2014)
 38. Lui, L.M., Wong, T.W., Zeng, W., Gu, X., Thompson, P.M., Chan, T.F., Yau, S.T.: Optimization of surface registrations using beltrami holomorphic flow. *Journal of scientific computing* **50**(3), 557–585 (2012)
 39. Lui, L.M., Zeng, W., Yau, S.T., Gu, X.: Shape analysis of planar multiply-connected objects using conformal welding. *IEEE transactions on pattern analysis and machine intelligence* **36**(7), 1384–1401 (2013)
 40. Ma, S., Goldfarb, D., Chen, L.: Fixed point and bregman iterative methods for matrix rank minimization (2009)
 41. Oreifej, O., Li, X., Shah, M.: Simultaneous video stabilization and moving object detection in turbulence. *IEEE Transactions on Pattern Analysis and Machine Intelligence* **35**(2), 450–462 (2013). DOI 10.1109/TPAMI.2012.97
 42. Peng, L., Huang, Z.Y., Jia, Y.Y.: Application of the combinatorial model of wavelet analysis and support vector machines in deformation analysis. *Proceedings of the 2nd International Conference on Remote Sensing, Environment and Transportation Engineering (RSETE)* pp. 1–4 (2012)
 43. Qiu, D., Lui, L.M.: Inconsistent surface registration via optimization of mapping distortions. *Journal of Scientific Computing* **83**(3), 1–31 (2020)
 44. Sobral, A., Bouwmans, T., ZahZah, E.: Double-constrained rpca based on saliency maps for foreground detection in automated maritime surveillance. In: 2015 12th IEEE International Conference on Advanced Video and Signal Based Surveillance (AVSS), pp. 1–6 (2015). DOI 10.1109/AVSS.2015.7301753
 45. Sotiras, A., Davatzikos, C., Paragios, N.: Deformable medical image registration: A survey. *IEEE Transactions on Medical Imaging* **32**(7), 1153–1190 (2013). DOI 10.1109/TMI.2013.2265603
 46. Taimouri, V., Hua, J.: Deformation similarity measurement in quasi-conformal shape space. *Graphical Models* **76**, 57–69 (2014)
 47. Tibshirani, R.: Regression shrinkage and selection via the lasso. *Journal of the Royal Statistical Society. Series B (Methodological)* **58**(1), 267–288 (1996). URL <http://www.jstor.org/stable/2346178>
 48. Tong, Y., Lombeyda, S., Hirani, A.N., Desbrun, M.: Discrete multiscale vector field decomposition. *ACM Trans. Graphics (TOG)* **22**, 445–452 (2003)
 49. Vercauteren, T., Pennec, X., Perchant, A., Ayache, N.: Diffeomorphic demons: Efficient non-parametric image registration. *NeuroImage* **45**(1, Supplement 1), S61 – S72 (2009). DOI <https://doi.org/10.1016/j.neuroimage.2008.10.040>. URL <http://www.sciencedirect.com/science/article/pii/S1053811908011683>. *Mathematics in Brain Imaging*
 50. Wang, Y., Lui, L.M., Gu, X., Hayashi, K.M., Chan, T.F., Toga, A.W., Thompson, P.M., Yau, S.T.: Brain surface conformal parameterization using riemann surface structure. *IEEE transactions on medical imaging* **26**(6), 853–865 (2007)
 51. Yao Jianchao: Image registration based on both feature and intensity matching. In: 2001 IEEE International Conference on Acoustics, Speech, and Signal Processing. *Proceedings (Cat. No.01CH37221)*, vol. 3, pp. 1693–1696 vol.3 (2001)
 52. Yasein, M.S., Agathoklis, P.: A feature-based image registration technique for images of different scale. In: 2008 IEEE International Symposium on Circuits and Systems, pp. 3558–3561 (2008)
 53. Ye, C.H., Yuan, X.M.: A descent method for structured monotone variational inequalities. *Optimization Methods and Software* **22**(2), 329–338 (2007). DOI 10.1080/10556780600552693. URL <https://doi.org/10.1080/10556780600552693>
 54. Yuan, X., Yang, J.: Sparse and low rank matrix decomposition via alternating direction method. *Pacific Journal of Optimization* **9** (2009)
 55. Zeng, W., Lui, L.M., Shi, L., Wang, D., Chu, W.C., Cheng, J.C., Hua, J., Yau, S.T., Gu, X.: Shape analysis of vestibular systems in adolescent idiopathic scoliosis using geodesic spectra. In: *International Conference on Medical Image Computing and Computer-Assisted Intervention*, pp. 538–546. Springer (2010)
 56. Zhou, T., Tao, D.: Godec: Randomized lowrank & sparse matrix decomposition in noisy case. pp. 33–40 (2011)
 57. Zhou, X., Yang, C., Yu, W.: Moving object detection by detecting contiguous outliers in the low-rank representation. *IEEE Transactions on Pattern Analysis and Machine Intelligence* **35**(3), 597–610 (2013). DOI 10.1109/TPAMI.2012.132
 58. Zitová, B., Flusser, J.: Image registration methods: a survey. *Image and Vision Computing* **21**(11), 977–1000 (2003). DOI [https://doi.org/10.1016/S0262-8856\(03\)00137-9](https://doi.org/10.1016/S0262-8856(03)00137-9). URL <https://www.sciencedirect.com/science/article/pii/S0262885603001379>